④

AFGL-TR-88-0093

TGAL-88-02

FINITE-DIFFERENCE MODELING OF RAYLEIGH WAVE SCATTERING AND P-SV(Lg) COUPLING PROBLEMS

Rong-Song Jih
Keith L. McLaughlin

Teledyne Geotech Alexandria Laboratories
314 Montgomery Street
Alexandria, VA 22314-1581

MARCH 1988

FINAL REPORT
FEBRUARY 1986 — FEBRUARY 1988

AIR FORCE GEOPHYSICS LABORATORY
AIR FORCE SYSTEMS COMMAND
UNITED STATES AIR FORCE
HANSCOM AIR FORCE BASE, MASSACHUSETTS 01731

DTIC
SELECTED
DEC 0 7 1988
H

88 12 6 048

HP A263 221

REPORT DOCUMENTATION PAGE

1a REPORT SECURITY CLASSIFICATION Unclassified	1b RESTRICTIVE MARKINGS
2a SECURITY CLASSIFICATION AUTHORITY	3 DISTRIBUTION/AVAILABILITY OF REPORT Approved for public release;
2b DECLASSIFICATION/DOWNGRADING SCHEDULE	Distribution unlimited.
4 PERFORMING ORGANIZATION REPORT NUMBER(S) TGAL-88-02	5 MONITORING ORGANIZATION REPORT NUMBER(S) AFGL-TR-88-0093

6a NAME OF PERFORMING ORGANIZATION Teledyne Geotech	6b OFFICE SYMBOL (If applicable) TGAL	7a NAME OF MONITORING ORGANIZATION Air Force Geophysics Laboratory
6c ADDRESS (City, State, and ZIP Code) 314 Montgomery Street Alexandria, VA 22314		7b ADDRESS (City, State, and ZIP Code) Hanscom AFB, MA 01731-5000

8a NAME OF FUNDING/SPONSORING ORGANIZATION Air Force Geophysics Lab.	8b OFFICE SYMBOL (If applicable) DSO/GSD	9. PROCUREMENT INSTRUMENT IDENTIFICATION NUMBER F19628-86-C-0054

8c. ADDRESS (City, State, and ZIP Code) Hanscom AFB, MA 01731-5000	10. SOURCE OF FUNDING NUMBERS			
	PROGRAM ELEMENT NO. 62714E	PROJECT NO. 6A10	TASK NO DA	WORK UNIT ACCESSION NO. BC

11. TITLE (Include Security Classification)

Finite-Difference Modeling of Rayleigh Wave Scattering and P-SV(Lg) Coupling Problems

12. PERSONAL AUTHOR(S)
Rong-Song Jih and Keith L. McLaughlin

13a TYPE OF REPORT Final Report	13b TIME COVERED FROM Feb 86 TO Feb 88	14. DATE OF REPORT (Year, Month, Day) March 1988	15. PAGE COUNT 64

16 SUPPLEMENTARY NOTATION

17 COSATI CODES			18 SUBJECT TERMS (Continue on reverse if necessary and identify by block number)
FIELD	GROUP	SUB-GROUP	Finite-Difference Method Rayleigh wave Lg wave Heterogeneity Topography Attenuation Scattering

19 ABSTRACT (Continue on reverse if necessary and identify by block number)

We briefly summarize in this final report the results from the two scientific reports delivered under contract F19628-86-C-0054. Our work has focused on the effects of near-source heterogeneity upon seismic wave scattering and phase conversions.

The basic tool in this work was a developing 2-dimensional explicit linear finite-difference code. By use of various initial conditions and/or the principle of reciprocity, we can generate the teleseismic response of the Earth model to a general seismic source. We have also modeled the propagation of Pn/Sn/Rg phases with some Arctic paths, without using the principle of reciprocity, under another contract. This FORTRAN-77 code has been run under the UNIX operating system on VAX, SUN, Convex, and Celerity computers. Major modifications of the code during the past two years include the addition of general free-surface boundary conditions capable of handling topography with inclined ramps of any slope, the fundamental mode Rayleigh wave packet adequate for both a homogeneous medium as well as a layered medium, and the grid-patching technique to eliminate the computer limitation on grid size. Work on this program continues to increase its performance, versatility, and to implement realistic earthquake sources. A user manual of Geotech's latest version of the finite-difference code is included in this report (cf. appendix).

20 DISTRIBUTION/AVAILABILITY OF ABSTRACT ☐ UNCLASSIFIED/UNLIMITED ☐ SAME AS RPT ☐ DTIC USERS	21 ABSTRACT SECURITY CLASSIFICATION Unclassified
22a NAME OF RESPONSIBLE INDIVIDUAL James F. Lewkowicz	22b TELEPHONE (Include Area Code) (617) 377-3028	22c OFFICE SYMBOL AFGL/LWH

Unclassified

(19. continued)

Rayleigh waves normally incident upon 2-D shallow heterogeneity are simulated by the linear finite-difference method to study attenuation, transmission, and reflection of Rayleigh waves and to measure the Rayleigh-to-P and -SV body wave conversion. Transmission, reflection, and scattering depend on the depth, average scale size of the heterogeneity, and the amplitude of the spatial fluctuation of velocity. As expected, larger spatial variation in velocity attenuates Rayleigh waves more than smooth media, and the attenuation is roughly proportional to the variance of the velocity fluctuation. The attenuation and scattering due to shallow heterogeneity is weaker than attenuation due to moderately rough topography.

Scattered body wave energy is studied as a function of frequency, scattering angle, and wave type (P or SV). Attenuation of Rayleigh waves by scattering from 2-D shallow velocity heterogeneity is dominated by conversion to body waves and in particular SV energy. Low frequency P and SV energy is scattered in a backwards direction, and high frequency P and SV energy is scattered in a forward direction.

As with scattering from rough topography, much of the converted SV energy will be trapped in the crustal waveguide at Lg phase velocities. Therefore, Rayleigh (Rg) to SV body wave conversion by shallow heterogeneity and topography should contribute to the formation of Lg by explosions, quarry blasts, and shallow earthquakes.

A comparison was made with results for P-coda from Greenfield (1971). The comparison indicates that self-similar and Gaussian models could be derived with rms velocity variations between 7 and 15% in the upper 3 km of the crust that would produce the observed P-coda/P power levels observed by Greenfield (1971).

Linear finite-difference (FD) method was used to compare the excitation of far-field P- and SV-waves generated by shallow dilatational sources in a suite of heterogeneous 2-D crustal models. The crustal models tested included simple layered structures, media with random velocity perturbations having Gaussian or self-similar autocorrelation functions, media with rough or gentle topography generated by Markov chains, and laminated media with sinusoidal folds. The numerical experiments were conducted by directing a broadband planar P- or SV-wave with appropriate incidence angle upon the testing models. The dilatational strain history at a shallow linear array of grid points was then recorded so that the far-field P- or SV(Lg)-waves from shallow dilatational sources could be inferred by use of the principle of reciprocity. The raw FD synthetics were deconvolved so as to represent the response due to explosion sources with a fixed yield. The mean peak amplitude of the synthetics for each model are compared to that for a reference model consisting of a simple layered medium. The average energy content in an appropriate signal window was measured as a complement to the amplitude measurement. Both approaches show essentially the same pattern of P/SV excitation, namely that models with topography consistently produce the strongest P-SV conversion among all types of crustal models. The introduction of interfaces (e.g., dipping layers) alone does not by itself increase SV excitation with the required slowness range. Thus $m_b(P) - m_b(Lg)$ appears to be smaller for models with topographic relief (e.g., the Degelen region of the central portion of the East Kazakh Test Site (EKTS)) than for models with dipping layers or folded sedimentary rocks (e.g., Shagan River, eastern EKTS). This result is quite different from Nuttli's (1987) observations based on WWSSN film chip readings of Lg, which suggest that $m_b(P) - m_b(Lg)$ varies from 0.036 ± 0.015 for the Shagan River area to 0.27 ± 0.03 for the Degelen area.

Recommendations for further work include:

(1) Extensions of the current finite-difference code from 2-D to 3-D to study the attenuation of body waves by 3-D heterogeneity in the crust, test hypotheses about the generation of P coda and anisotropic P wave generation, and generation of transverse Lg by explosions.

(2) Introduction of other numerical methods to explore the coupling (scattering) of modes of wave-guide regional phases such as Pg and Lg, as well as the scattering of Pn and Sn. These methods include 2-D and 3-D scattering from localized heterogeneity as well as from rough boundaries.

(3) Coupling of efficient reflectivity methods to finite difference calculations to propagate the scattered field to regional distances and to drive the finite difference responses with realistic in-coming regional phases.

(4) Investigation of scattering of fundamental and higher mode short-period Rayleigh waves by 2-D topography and shallow heterogeneity with more realistic velocity gradients near the surface.

(5) Extension of the general topographic boundary condition to include the general fluid-solid interface for the modeling of scattering at rough fluid-solid boundaries.

(6) Improvement of the polygonal free-surface boundary conditions for higher precision.

TABLE OF CONTENTS

(THIS PAGE INTENTIONALLY LEFT BLANK)

CONTRIBUTING SCIENTISTS

The following research staff of Alexandria Laboratories contributed to research performed during the period covered by this contract:

Keith L. McLaughlin   Geophysicist, Former Principal Investigator
Rong-Song Jih   Mathematician, Acting Principal Investigator

REPORTS AND PUBLICATIONS GENERATED DURING FEB 86 - FEB 88

McLaughlin, K. L., L. M. Anderson, and A. C. Lees (1987), Effects of geologic structure on Yucca Flats, NTS, explosion waveforms: 2-dimensional linear finite-difference simulations, *Bull. Seism. Soc. Am.*, 77, 1211-1222.

McLaughlin, K. L., and R.-S. Jih (1987), Finite-difference simulations of Rayleigh wave scattering by 2-D rough topography (submitted to *Bull. Seism. Soc. Am.*).

McLaughlin, K. L., and R.-S. Jih (1987), Finite-difference simulations of Rayleigh wave scattering by shallow heterogeneity, *Report AFGL-TR-87-0322 (TGAL-87-02)*, Teledyne Geotech, Alexandria, VA 22314.

Jih, R.-S., and K. L. McLaughlin (1988), Investigation of explosion generated SV Lg waves in 2-D heterogeneous crustal models by finite-difference method, *Report AFGL-TR-88-0025 (TGAL-88-01)*, Teledyne Geotech, Alexandria, VA 22314.

Jih, R.-S., K. L. McLaughlin, and Z. A. Der (1988), Free boundary conditions of arbitrary polygonal topography in a 2-D explicit elastic finite-difference scheme, *Geophysics*, 53, 1045-1055.

McLaughlin, K. L., and R.-S. Jih (1988), Scattering from near-source topography: teleseismic observations and numerical 2-D explosive line sources simulations, *Bull. Seism. Soc. Am.*, 78 1399-1414.

SUMMARY OF RESEARCH COMPLETED DURING FEB 86 - FEB 88

FD Simulations of Rayleigh Wave Scattering by Shallow Heterogeneity

Rayleigh waves normally incident upon 2-D shallow heterogeneity are simulated by the linear finite-difference method to study attenuation, transmission, and reflection of Rayleigh waves and to measure the Rayleigh-to-P and -SV body wave conversion (cf. AFGL-TR-87-0322, also Figures 1, 2, and 3). Transmission, reflection, and scattering depend on the depth, average scale size of the heterogeneity and the amplitude of the spatial fluctuation of velocity. As expected, larger spatial variation in velocity attenuates Rayleigh waves more than smooth media, and the attenuation is roughly proportional to the variance of the velocity fluctuation (Figures 4 and 5). The attenuation and scattering due to shallow heterogeneity is weaker than attenuation due to moderately rough topography.

Scattered body wave energy is studied as a function of frequency, scattering angle, and wave type (P or SV). Attenuation of Rayleigh waves by scattering from 2-D shallow velocity heterogeneity is dominated by conversion to body waves and in particular SV energy. Low frequency P and SV energy is scattered in a backwards direction, and high frequency P and SV energy is scattered in a forward direction.

As with scattering from rough topography, much of the converted SV energy will be trapped in the crustal waveguide at Lg phase velocities. Therefore, Rayleigh (Rg) to SV body wave conversion by shallow heterogeneity and topography should contribute to the formation of Lg by explosions, quarry blasts, and shallow earthquakes.

A comparison is made with results for P-coda from Greenfield (1971).[1] The comparison indicates that self-similar and Gaussian models could be derived with rms velocity variations between 7 and 15% in the upper 3 km of the crust that would produce the observed P-coda/P power levels observed by Greenfield (1971) (Figure 6).

---

[1] Greenfield, R. J. (1971), Short-period P-wave generation by Rayleigh-wave scattering at Novaya Zemlya, *J. Geophys. Res.*, 76, 7988-8002.
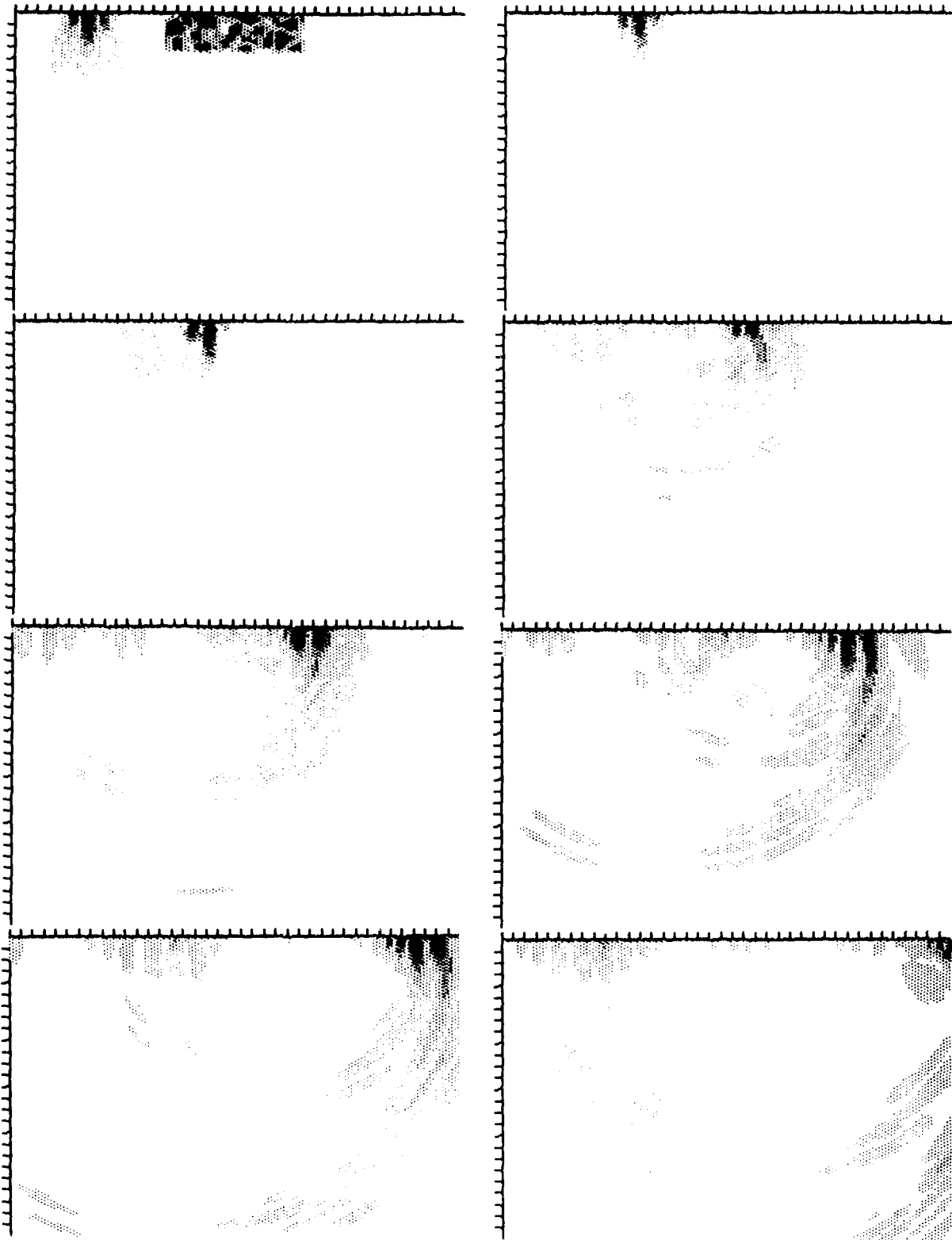
Figure 1. The snapshots of the displacement field due to Rayleigh wave propagating in a medium with shallow heterogeneity of $v = 10\%$, $a = 1km$, $h = 3.2km$. Successive frames are separated by 2 sec intervals. Displacements are proportional to the darkness of the plot and are normalized to the maximum in each frame.
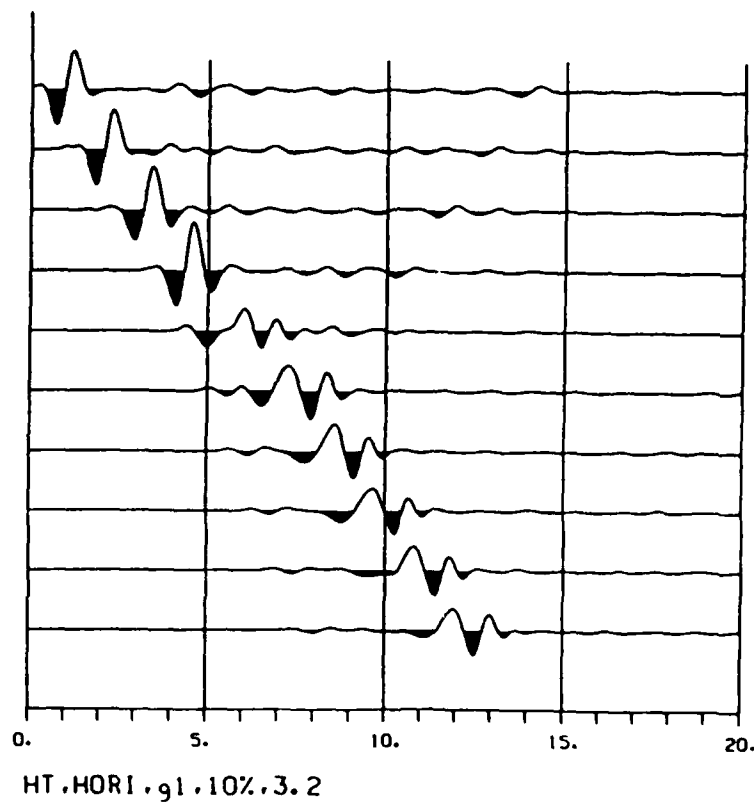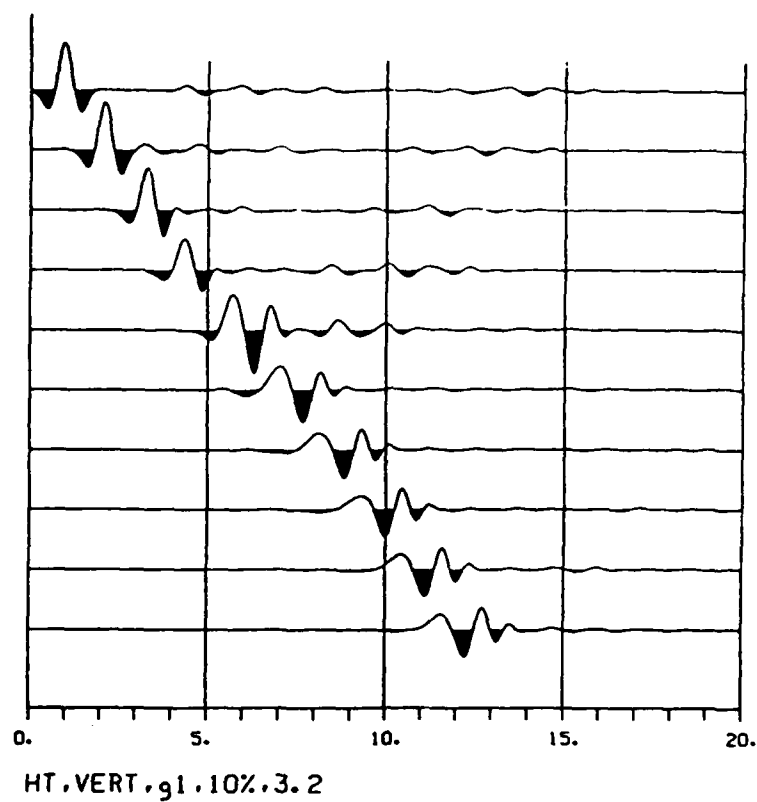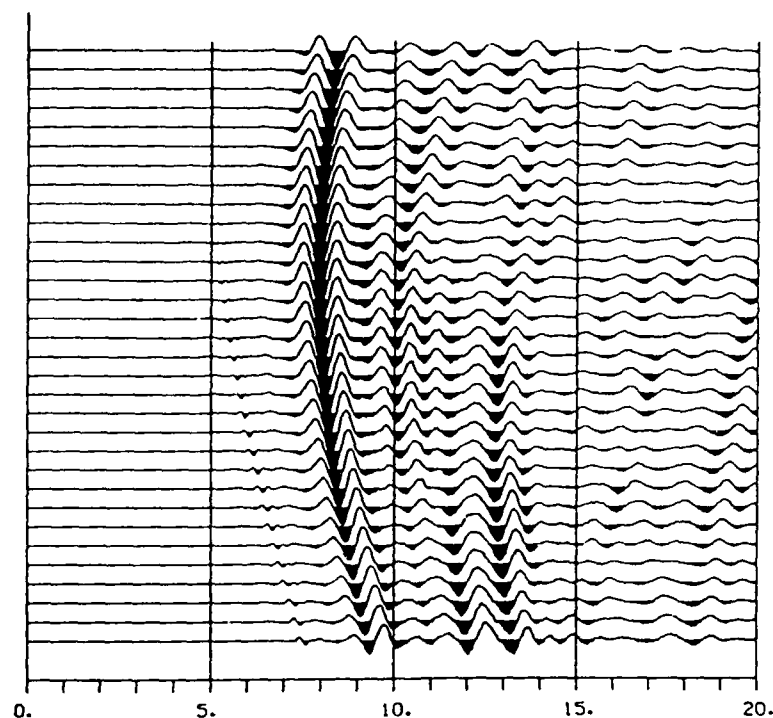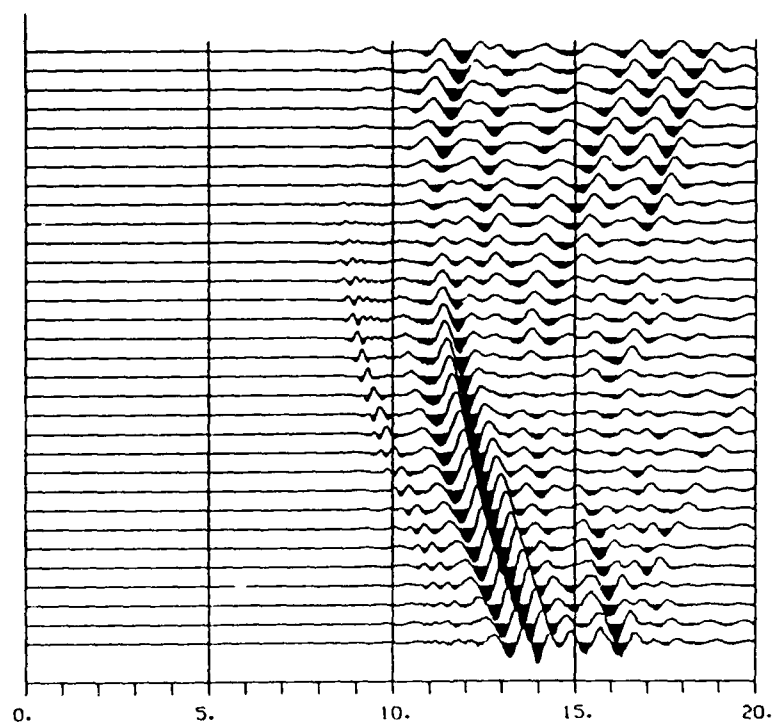
HT,VERT,g1,10%,3.2

HT.HORI,g1,10%,3.2

Figure 2. Synthetic near-surface vertical displacements (upper) and horizontal displacements (below) for a Rayleigh wave propagating in a medium with shallow heterogeneity of $v = 10\%$, $a = 1$km, $h = 3.2$km.

deepDILA.1km.g=1.10%.3.2

deepROTA.1km.g=1.10%.3.2

Figure 3. Seismic sections recording the converted P wave (dilatational strain, upper) and S wave (rotational strain, lower) at a line of 32 sensors near the bottom of the grid spaced 1 km apart for the case of v = 10%, a = 1km, h = 3.2km. See Figure 1 for snapshots.
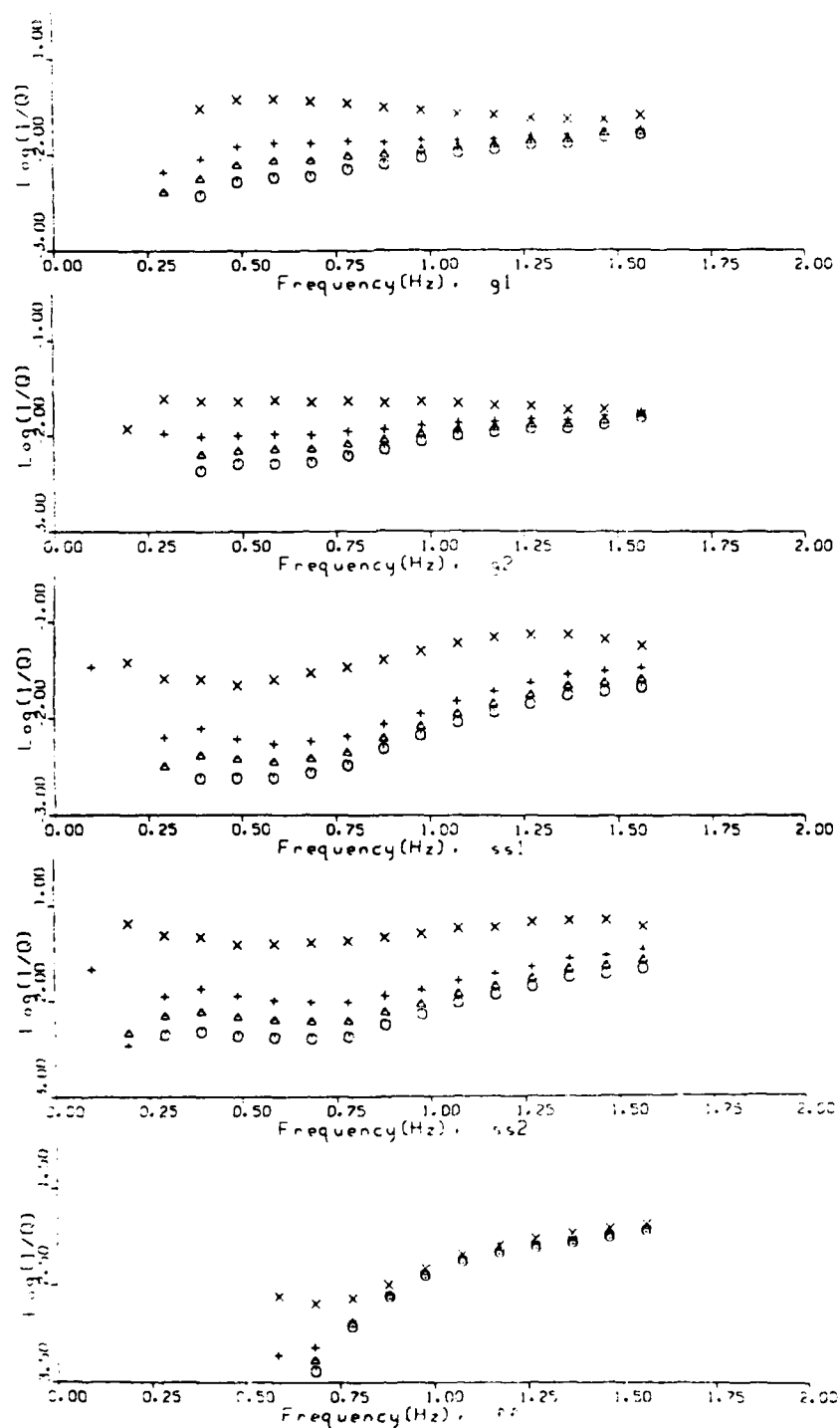
LOSS DUE TO HETEROGENEITY

Figure 4. Attenuation factor observed as a function of frequency from the FD simulations. "x", "+", triangles, and circles correspond to fluctuation of P wave velocity v = 20%, 10%, 7%, and 5% respectively. The shallow heterogeneous media tested are (from top to bottom): 4 Gaussian media with a = 1km, h = 3.2km; 4 Gaussian media with a = 2km, h = 3.2km; 4 self-similar media with a = 1km, h = 3.2km; 4 self-similar media with a = 2km, h = 3.2km; folded sinusoidal layers with h = 3.2km, λ = 2km, peak-to-peak amplitude 2.5km.
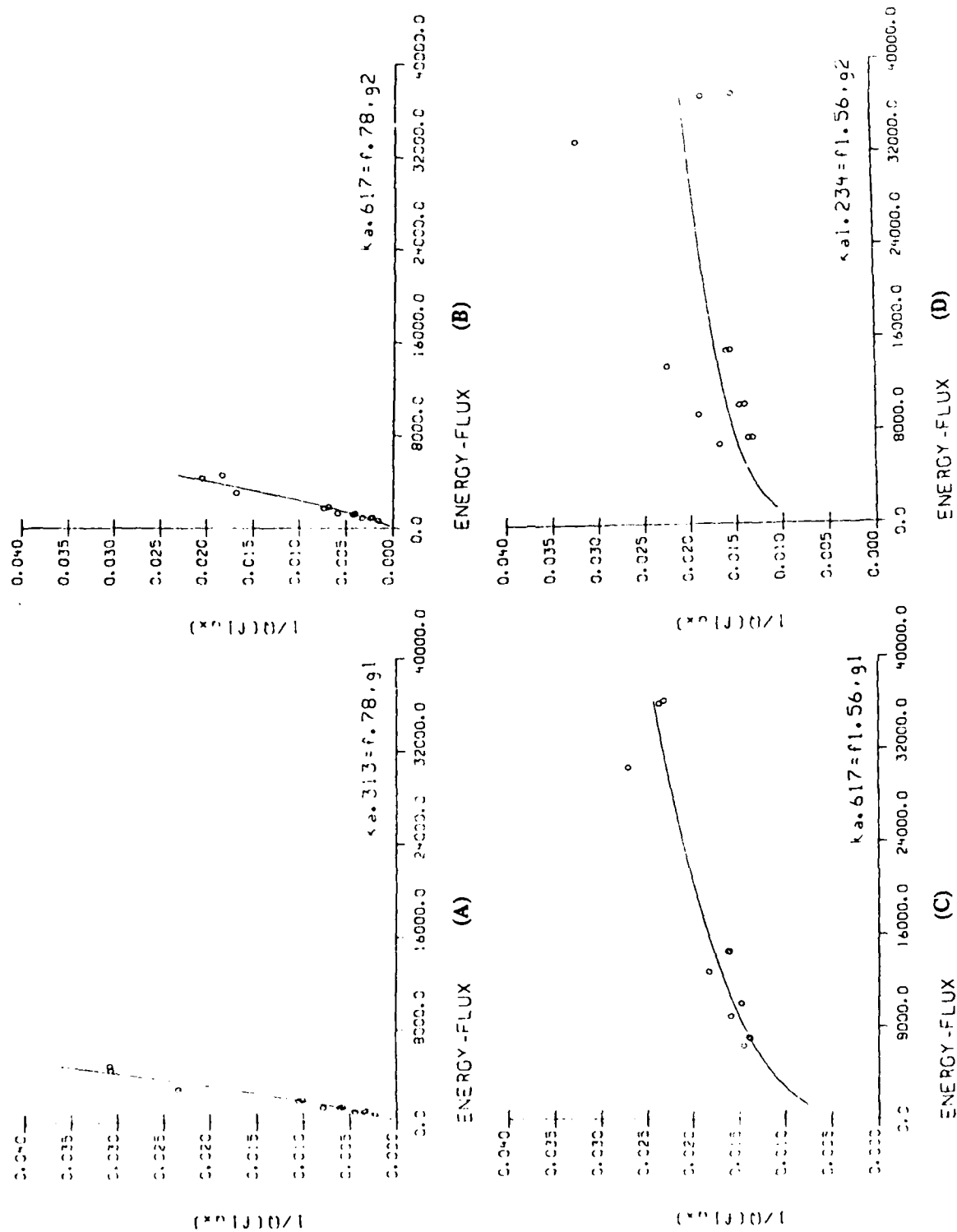
Figure 5. The attenuation factor 1/Q at 0.78 Hz and 1.56Hz versus energy-flux ξ of Gaussian models of various thickness (1km, 2km, and 3.2km) and velocity fluctuations ($v = 5\%$, 7%, 10% and 20%). (A) 0.78Hz, a=1, fitted to curve $\Gamma = \Gamma_o \xi^{1.2842}$, 0.78Hz, a=2, fitted to curve $\Gamma = \Gamma_o \xi^{1.299}$, (C) 1.56 Hz, a=1, fitted to curve $\Gamma = \Gamma_o \xi^{0.3434}$, (D) 1.56 Hz, a=2, fitted to curve $\Gamma = \Gamma_o \xi^{0.1944}$.
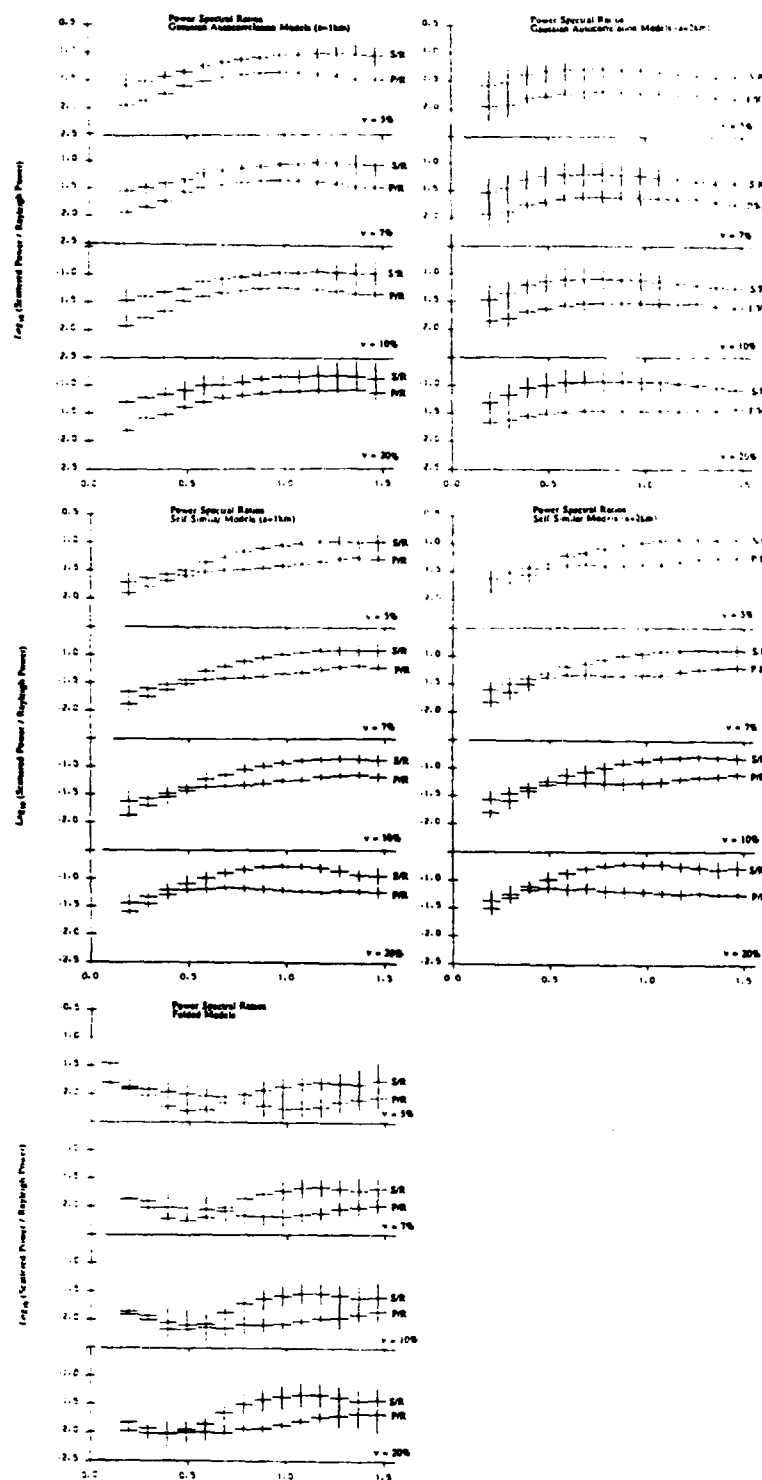
Figure 6. Power spectral ratios of the scattered P and S waves to the incident Rayleigh wave of various models. Units are $3.4*10^{-5}$ and $1.2*10^{-5}$ *erg/sec/cm³/(cm* of heterogeneity)/(cm² incident Rayleigh wave) for the P-wave and S-wave coda power density at a depth of 3.2 km in the grid. P-wave coda is lower set of values, S-wave coda is upper set of values. (A) Gaussian autocorrelation models (a= 1 km, h = 3.2 km), v varies from 20% (top), 10%, 7%, to 5% (bottom). (B) Same as (a) except a= 2 km. (C) Self-similar autocorrelation models with a= 1 km. (D) Self-similar autocorrelation models with a= 2 km. (E) Folded models.

SUMMARY OF RESEARCH COMPLETED DURING THE PERIOD MAY 87 TO FEB 88

FD Studies of P-SV(Lg) Coupling in 2D Crustal Models

A linear finite-difference (FD) method has been used to compare the excitation of far-field P- and SV-waves generated by shallow dilatational sources in a suite of hypothetical heterogeneous 2-D crustal models (cf. AFGL–TR–88–0025). The crustal models tested included simple layered structures, media with random velocity perturbations having Gaussian or self-similar autocorrelation functions, media with rough or gentle topography generated by Markov chains, and laminated media with sinusoidal folds. The numerical experiments were conducted by directing a planar P- or SV-wave with appropriate incidence angle upon the testing models (Figures 7 and 8). The dilatational strain history at a shallow linear array of grid points was then recorded so that the far-field P- and SV(Lg)-waves from shallow dilatational sources could be inferred by using the principle of reciprocity. The raw FD synthetics were deconvolved so as to represent the response due to explosion sources with a fixed yield (Figure 9). The mean peak amplitudes of the synthetics for each model are compared to that for a reference model consisting of a simple layered medium. The average energy content in an appropriate signal window was measured as a complement to the amplitude measurement (Figure 10). Both the amplitude and energy measurements show essentially the same pattern of P/SV excitation, namely that models with topography consistently produce the strongest P-SV conversion among all types of crustal models (Tables 1 and 2). The introduction of interfaces (e.g., dipping layers) alone does not by itself increase SV excitation with the required slowness range. Thus $m_b(P) - m_b(Lg)$ appears to be smaller for models with topographic relief than for models with dipping layers or folded sedimentary rocks.

These synthetic results are consistent with observations for Novaya Zemlya (Nuttli,

1988)[2] and Shagan River (Nuttli, 1986),[3] based on WWSSN film chip readings of Lg. Novaya Zemlya, which has rough topography, shows relatively higher Lg with respect to P ($m_b(P)$ - $m_b(Lg)$ = -0.11) than does the somewhat flatter Shagan River test site ($m_b(P)$ - $m_b(Lg)$ = 0.04). However, Nuttli (1987)[4] also obtained an even lower value of Lg relative to P ($m_b(P)$ - $m_b(Lg)$ = 0.27) for the Degelen Mountain test site, only 70 km away from Shagan River. If this Degelen-Shagan bias is real, then it must be due to near-source effects, and these cannot be explained by the FD results obtained to date. However, some recently archived high-quality digital seismograms recorded at the Chinese Digital Seismic Network indicate more Lg excitation (with respect to P) at Degelen than at Shagan River (Figure 13), which is consistent with the numerical results (Figures 11 and 12).

The finite-difference results also show negatively correlated P and SV energy (Figures 11 and 12), which provides a preliminary explanation of the success of the unified yield estimator. Measuring all possible phases tends to reduce the effects of uneven energy release on source size estimation. To understand this issue in a more quantitative manner, and to derive an optimal weighting scheme to combine all phases, theoretical studies with numerical simulations on detailed deterministic (rather than oversimplified or hypothetical) models of the Soviet test sites are necessary.

---

[2] Nuttli, O. W. (1988), Lg magnitudes and yield estimates for underground Novaya Zemlya nuclear explosions, *Bull. Seism. Soc. Am.*, 78, 873-884.

[3] Nuttli, O. W. (1986), Lg magnitudes of selected East Kazakhstan underground explosions, *Bull. Seism. Soc. Am.*, 76, 1241-1251.

[4] Nuttli, O. W. (1987), Lg magnitudes of Degelen, East Kazakhstan, underground explosions, *Bull. Seism. Soc. Am.*, 77, 679-681.

TABLE 1. AMPLITUDE COMPARISON OF P AND SV Lg EXCITATION			
model	P	Lg	P-Lg	Description of the model
0	0.000	0.000	0.000	reference model (1-uniform layer, 5+0%, 2km thick)
1	-0.207	0.202	-0.409	rough TOPO + 1 uniform layer (5+0%, 2km thick)
2	-0.006	0.132	-0.139	gentle TOPO + self-similar layer (5+10%, 2km)
3	-0.196	0.110	-0.305	rough TOPO + Gaussian layer (5+10%, 2km)
4	-0.023	0.073	-0.096	gentle TOPO + 1 uniform layer (5+0%, 2km)
5	-0.034	0.044	-0.078	self-similar layer (5+10%, 2km thick)
6	-0.162	0.019	-0.181	folded sinusoidal layers (L=2,H=2.5,5+20%)
7	-0.031	0.014	-0.045	folded sinusoidal layers (L=2,H=2.5,5+10%)
8	-0.134	-0.037	-0.098	self-similar layer (5+20%, 2km thick)
9	-0.029	-0.037	0.008	folded sinusoidal layers (L=5,H=2.5,5+10%)
10	0.003	-0.058	0.061	2-Gaussian layer (4.5+10%/5+10%, total 2km)
11	0.019	-0.091	0.110	steeply dipping layers (52°)
12	0.011	-0.093	0.104	gently dipping layers (26°)
13	0.018	-0.137	0.155	steeply dipping layers (-52°)
14	0.009	-0.143	0.152	gently dipping layers (-26°)

TABLE 2. COMPARISON OF P AND SV Lg SPECTRAL CONTENT ON 0.5-1.0 Hz			
model	P	Lg	P-Lg	Description of the model
0	0.000	0.000	0.000	reference model (1-uniform layer, 5+0%, 2km thick)
1	-0.400	0.083	-0.483	rough TOPO + uniform layer (5+0%,2km)
2	-0.049	0.057	-0.106	gentle TOPO + self-similar layer(5+10%,2km)
3	-0.363	0.063	-0.426	rough TOPO + Gaussian layer (5.0+10%,2km)
4	-0.180	0.019	-0.199	gentle TOPO + uniform layer (5+0%,2km)
5	0.016	0.009	0.007	self-similar layer (5+10%,2km)
6	0.099	-0.031	0.130	folded sinusoidal layers (5+20%,L=2,H=2.5)
7	0.058	-0.101	0.159	folded sinusoidal layers (5+10%,L=2,H=2.5)
8	-0.026	-0.049	0.023	self-similar layer (5+20%,2km)
9	0.015	-0.163	0.178	folded sinusoidal layers (5+10%,L=5,H=2.5)
10	0.083	-0.007	0.090	2-Gaussian layer (4.5+10%/5.0+10%,2km)
11	-0.008	-0.048	0.040	steeply dipping layers (52°)
12	-0.024	-0.057	0.033	gently dipping layers (26°)
13	0.015	-0.086	0.101	steeply dipping layers (-52°)
14	-0.001	-0.103	0.102	gently dipping layers (-26°)

12.5km

12.5km   0 sec   1 sec
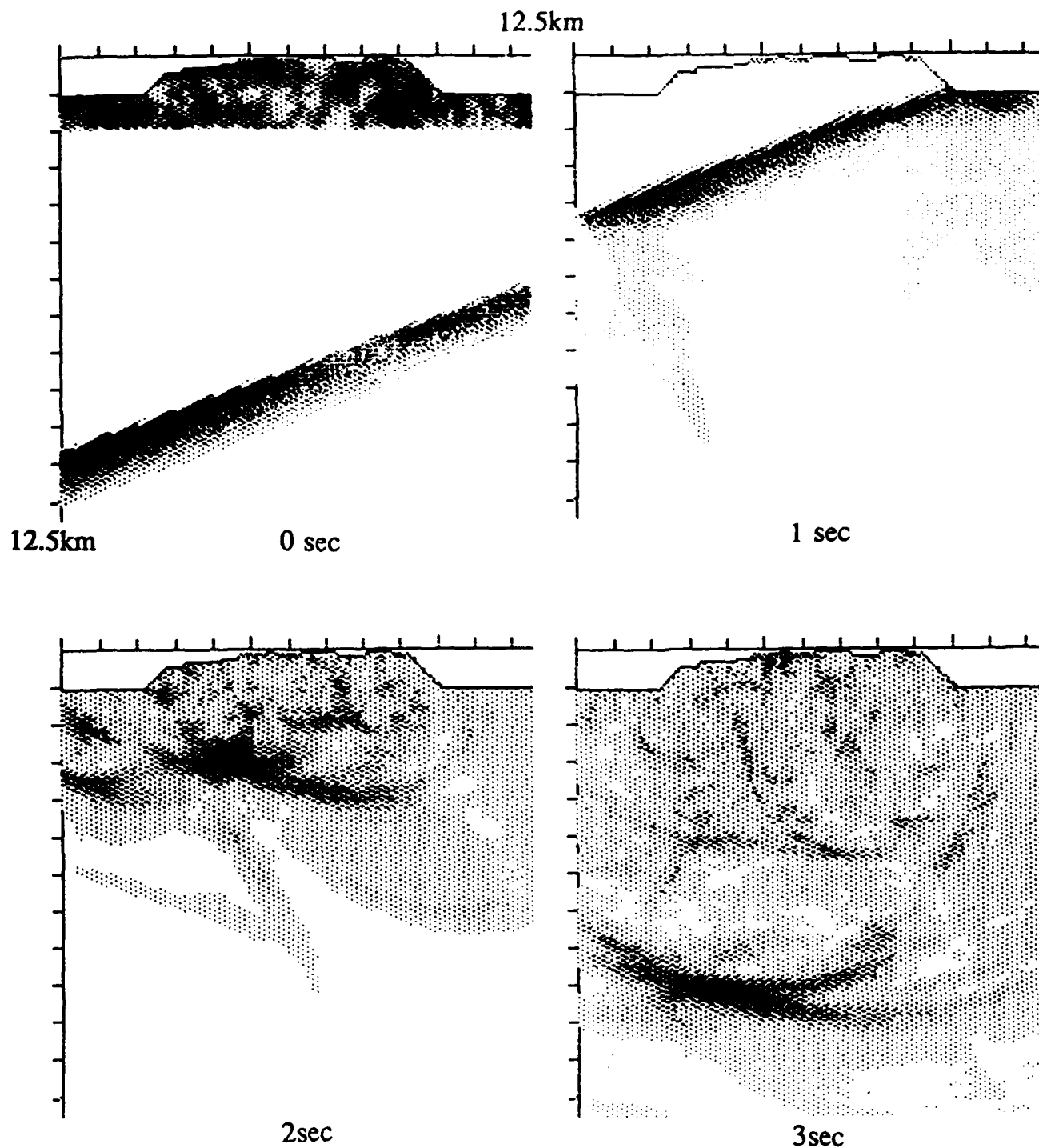
2sec   3sec

Figure 7. P wave in a half space (α = 6.0 km/s, β = 3.55 km/s) incident at $20°$ upon a 2 km layer with average P-wave velocity of 5 km/s and a self-similar 10% rms velocity variation superimposed by a gentle topography (indicated in the 0 sec frame, also model 2 in Tables 1 and 2) The S-wave velocity is assumed to be proportional to the P-wave velocity. Darkness of the snapshots are proportional to the displacement amplitude. Snapshots of the displacement field are shown at 1 second intervals. The dilatational strain is recorded at 32 locations at a depth of 0.5 km in order to infer the excitation of far-field P waves from explosion sources. Although absorbing boundary conditions are used, care must be taken to avoid residual reflections from the sides of the grid.
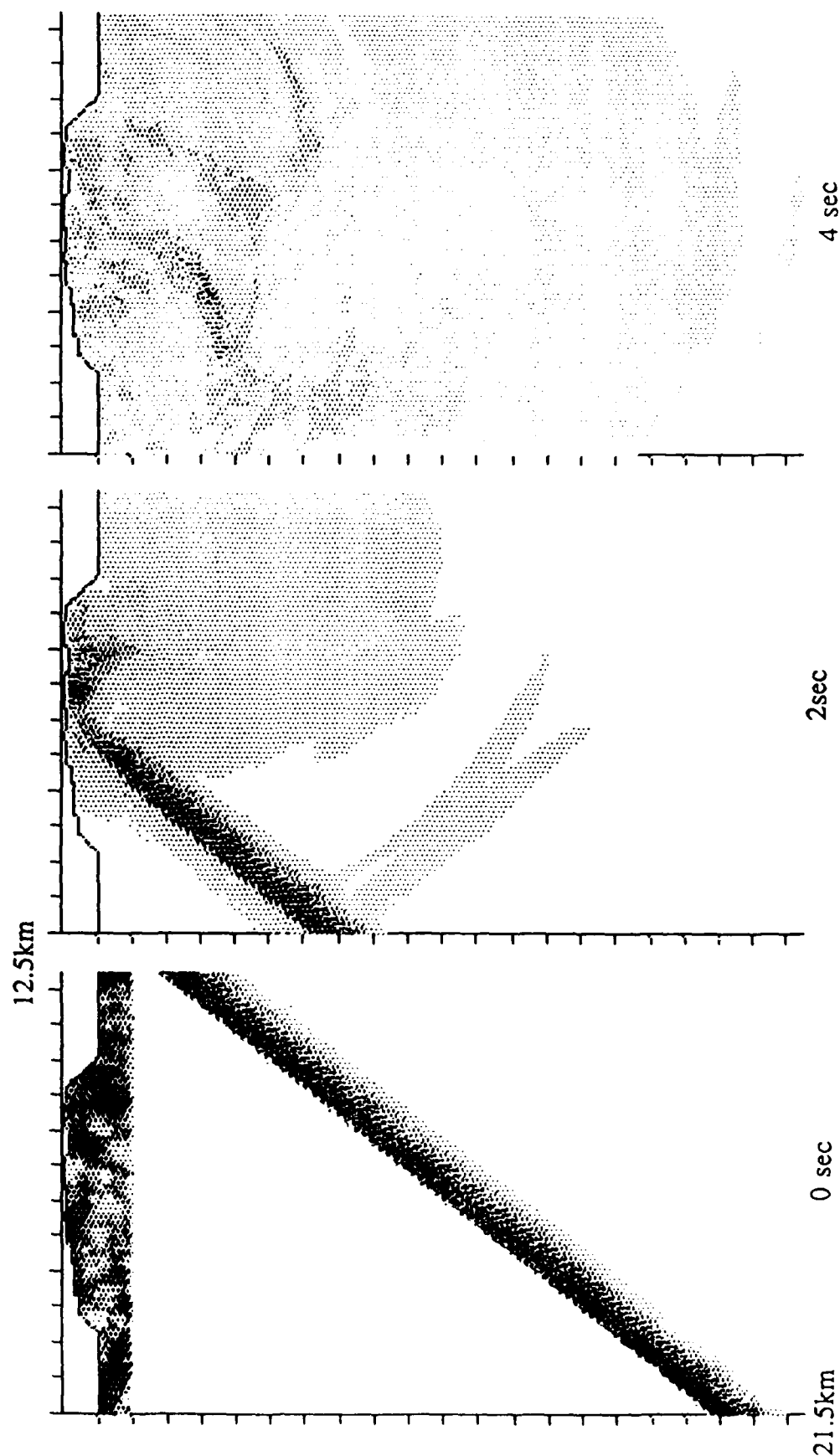
Figure 8. S wave in a half space (α = 6.0 km/s, β = 3.55 km/s) incident at 52° upon a 2 km self-similar layer with average P-wave velocity of 5 km/s and 10% rms velocity variation superimposed by a gentle topography (indicated in the 0 sec frame, also model 2 in Tables 1 and 2). The dilatational strain is recorded at 32 locations at a depth of 0.5 km in order to infer the excitation of far-field S waves from explosion sources.
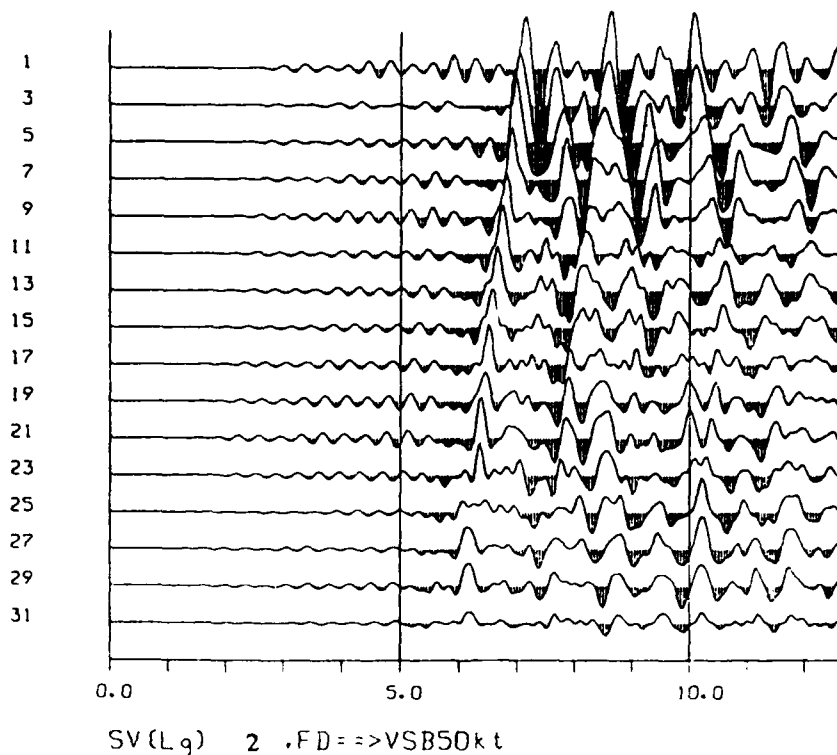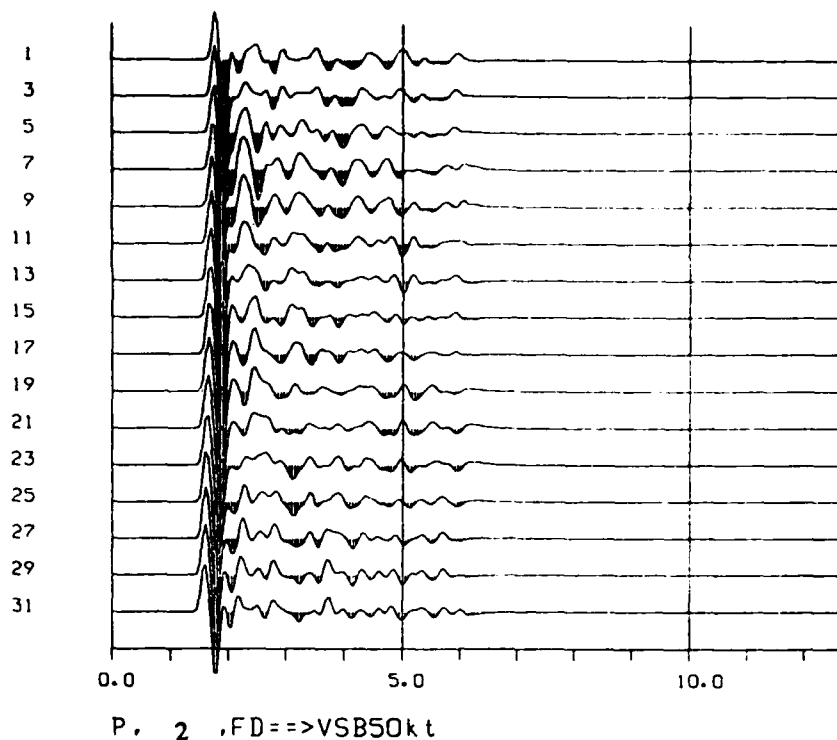
P, 2 ,FD==>VSB50kt

SV(Lg) 2 .FD==>VSB50kt

Figure 9. Synthetic far-field P- (top) and SV-wave (bottom) inferred by the principle of reciprocity for model 2. The original dilatational strain history (5 Hz low-pass) responding to incident broadband P or SV plane wave recorded at 32 locations at 0.5 km depth in the reference model. Shown here are the deconvolved synthetics corresponding to VSB 50 KT in hard rock. The peak amplitude of these synthetics was measured and compared to the average peak amplitude of the reference model.
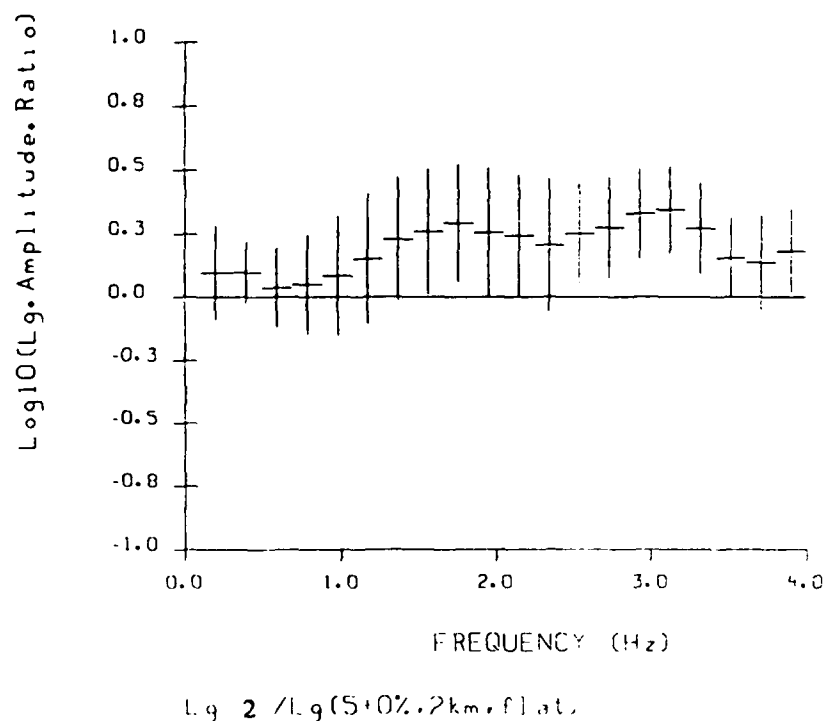
P 2 /P(S+0%.2km.flat)

Lg 2 /Lg(S+0%.2km.flat)
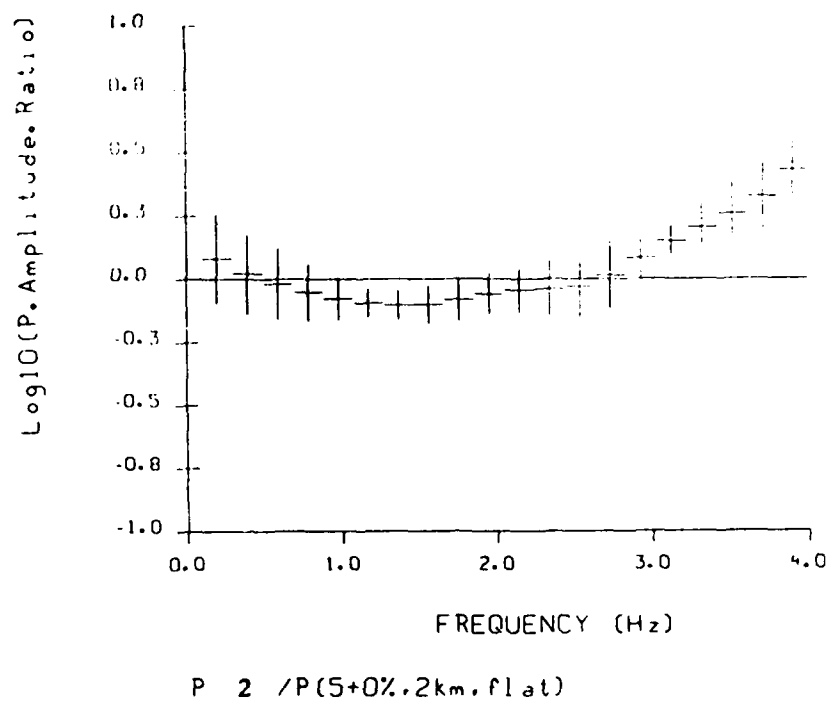
Figure 10. Average spectral ratio as a function of frequency, $Log(P_1/P_0)$ (upper) and $Log(Lg_1/Lg_0)$ (lower), of the Model 2 relative to the reference model. P wave response of model 1 in the 0.5 to 1.0 Hz range is deficient with respect to the reference model by 0.348 log units, while the S wave response is 0.063 log unit above the reference model. Vertical bars represent the standard error of a single observation.
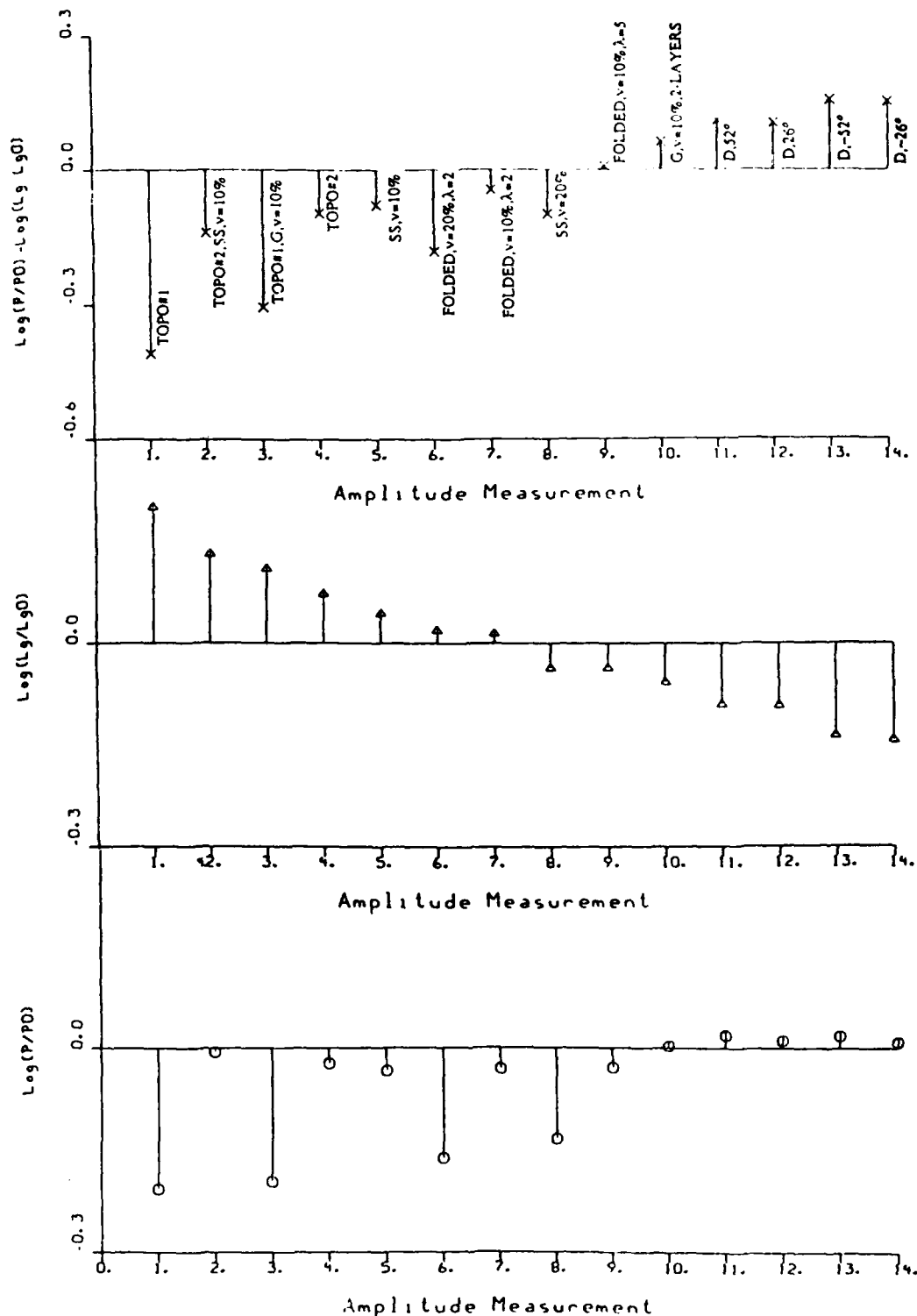
Figure 11. Averaged P and SV(Lg) peak amplitudes of array of shallow explosions in fourteen crustal models sorted with the $\log_{10}(Lg/Lg_0)$ values. Several observations are obvious: (1) Dipping layers (models 11 through 14) generate smaller Lg than the normalizing model, while they all generate more P than the reference model. (2) Media with topography (e.g. models 1 through 4) which represent CEKTS all generate more Lg than the normalizing model, while they excite less P due to strong P to S conversion. (3) Dipping layers (models 11 through 14) are more efficient than all other models for P excitation. Thus $m_b(P)$ and $m_b(Lg)$ appear to be negatively correlated.
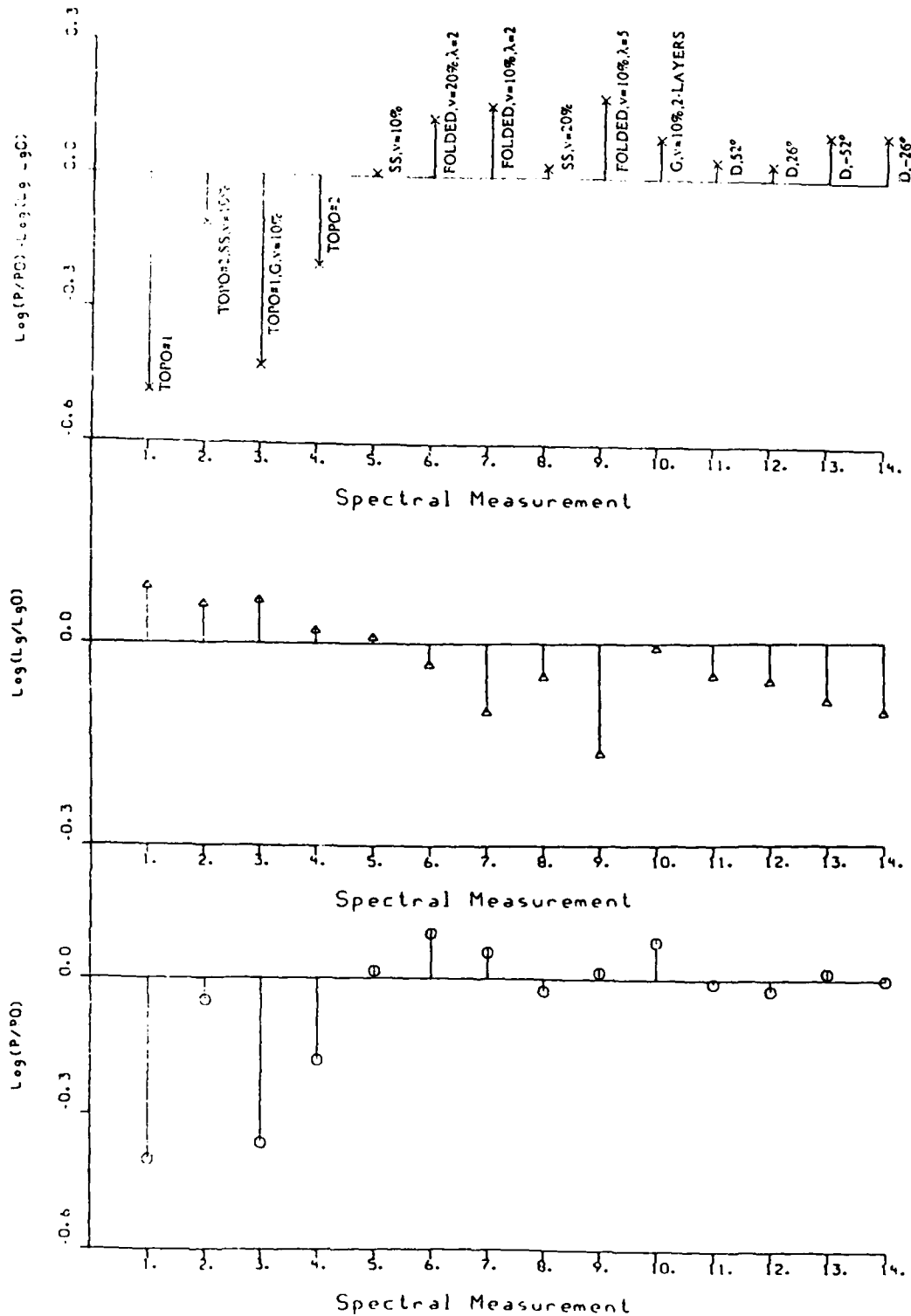
Figure 12. Same as Figure 11 except the P and SV(Lg) excitations are measured with the averaged spectral content in [0.5,1] Hz band. Crustal models with topography generate more Lg and less P than models with dipping layers, same as the result derived from peak amplitude measurement.
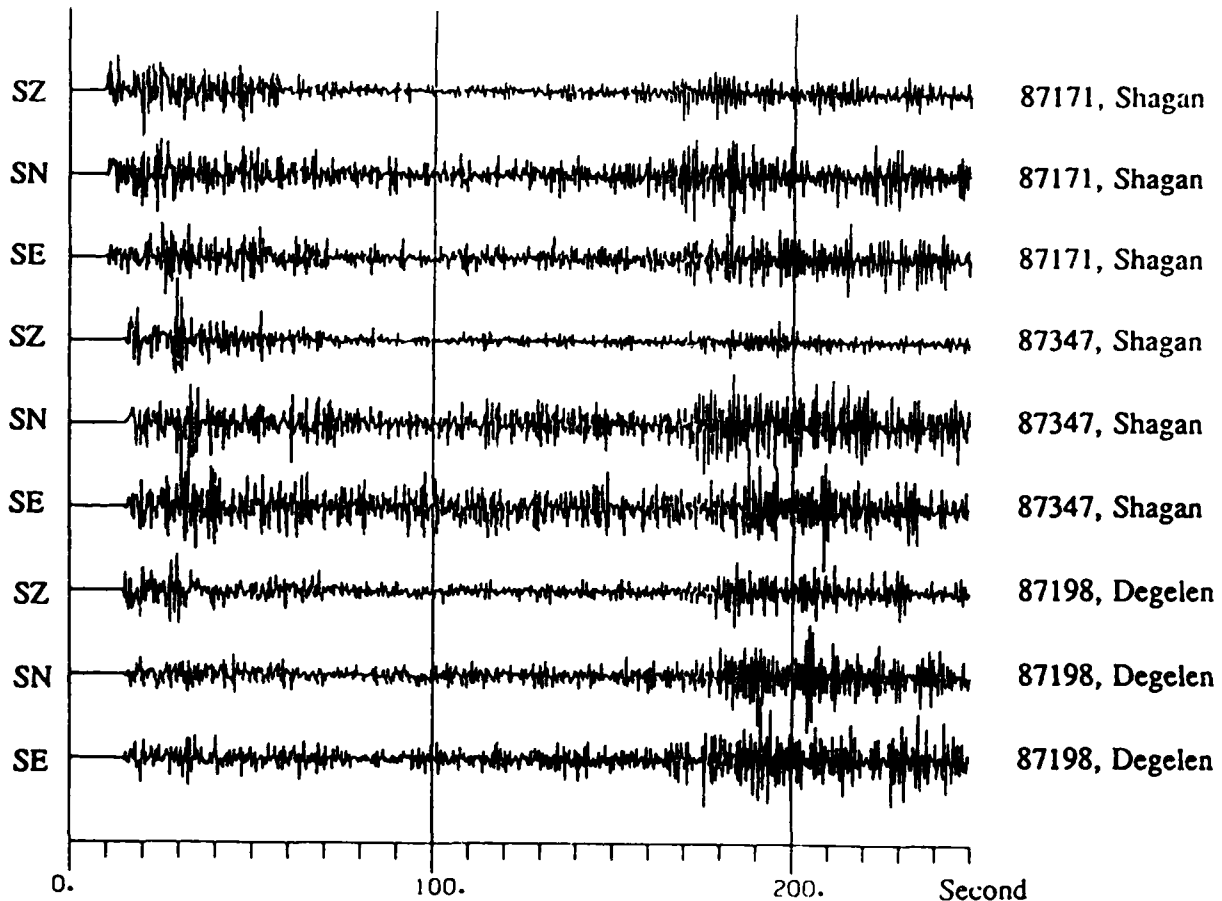
E. Kazakh Events, CDSN-WMQ

Figure 13. Short period seismograms of two Shagan events 87171 (78.74E, 49.91N, mb=6.1) and 87347 (78.85E, 49.96N, mb=6.1), and a Degelen event 87198 (78.11E, 49.80N, mb=5.8) recorded at CDSN station WMQ. Each trace is scaled by the peak amplitude. Note the relatively less P energy (with respect to Lg energy) in the Degelen event 87198 as compared to Shagan events of similar magnitudes. This observation is consistent with the finite-difference experiments (cf., Tables 1, 2 and Figures 11, 12).

DISCUSSION AND SUGGESTIONS

We see that moderate heterogeneity in a half space does not attenuate short-period fundamental Rayleigh waves nearly so much as rough topography does, but it can still contribute substantial P-coda and moderate attenuation of Rg. For the Gaussian media used in these simulations, the energy lost due to body wave conversion varies from several percent to 20% in 12 km distance. A significant result of the simulations is that reflection of Rayleigh waves by heterogeneity at normal incidence is in most cases inefficient, as was the case for rough topography. The only exception observed was a folded structure with a resonant response to the incident Rayleigh wave. Therefore we should not expect to see Rayleigh-wave back-scattering as a significant contributor to the multiple scattering of fundamental Rayleigh waves that populate coda for Gaussian or self-similar media. Backscattering can be significant for media with well defined organ-ized structures such as folded sedimentary structures. In such a case the backscattered wave has a narrow narrow bandwidth reflecting the resonance phenomenon.

More complicated random media contain many scale lengths and introduce broad-band effects. The Rayleigh-wave attenuation is a complicated function of frequency, but it attains a maximum in the range where the characteristic wavelength of the medium matches the wavelength of the incident Rayleigh wave.

At low frequency ($\lambda > a$) the coda dilatational and rotational wavenumber spectra indicate that the scattered P and SV waves are scattered in the forward direction except for strongly folded structures or Gaussian medium with very strong velocity fluctuations (20%). For higher frequencies ($\lambda < a$), the scattered body waves are always maximum in

the forward direction. A detailed analysis of Rayleigh to P-coda scattering will have to take this effect into account with an effective radiation pattern to the "equivalent scatterer".

The results presented in *AFGL-TR-87-0322* offer a beginning approach to understanding the effects upon surface waves of scattering by lateral heterogeneity. A complete exploration of the problem will require variation of the P and S velocities, near surface velocity gradients, and crustal velocity heterogeneity as a function of depth. Much of the SV energy scattered by near surface heterogeneities is concentrated at apparent velocities within 150% of the Rayleigh phase velocity. A crust with surface layer with $\beta = 2.96$ km/sec, as was used in these simulations, would leak much of the energy to the mantle. However, if the near-surface velocity of the model is lowered, then the slowness space occupied by the scattered waves will scale to the Rayleigh phase velocity, and more energy will be trapped in the crust. Other ways of increasing the trapping of the scattered SV energy are increasing the α/β ratio in the near surface, introduction of gradients near the surface to create higher order modes, and introduction of deeper velocity heterogeneity to scatter P and SV energy back into the waveguide. In short, all these mechanisms can act only to increase the Rayleigh-to-Lg coupling. Therefore, we expect that in real seismological situations much of the Rayleigh-wave energy scattered into SV by near-surface heterogeneity will be trapped in the crust and will find a path to the Lg wavepacket.

In our simplistic attempt to model SV-Lg excitation due to near-source heterogeneity scattering effects *(AFGL-TR-88-0025)*, we found that the total variance of the spectra of the teleseismic P wave was greater than the variance of the P-SV-Lg excitation (with the

slowness we investigated). Although we found that different geologic models gave different coupling, the variance was always larger for P than for P-SV for any models. This may explain Nuttli's claim that Lg is a stable estimator in a fixed geologic setting.

While we continue to experiment with various models, our preliminary results indicate that P to SV conversion is strongly enhanced by velocity variation in the vicinity of rough topography and by the introduction of low velocity layers near the surface. The introduction of interfaces alone does not of itself increase SV excitation with the required slowness range. We continue to experiment with the geometry of heterogeneity and with the scale lengths of the heterogeneity. Although we cannot presently explain Nuttli's (1987) results, we predict substantial variations in SV Lg excitation by explosions embedded in crustal heterogeneity. It seems that P-to-SV is not the only mechanism for explosion Lg excitation, so it is necessary to investigate the excitation of SH(Lg) as well.

A possibility is that Nuttli's m_b:Lg relationship might be related to Rayleigh-to-P conversion away from the immediate location of the source. Our numerical simulations treated only the P-S conversions that might occur within a few km of the source, given some simple models. If either the Rayleigh excitation or the Rayleigh scattering is different for CEKTS and EEKTS, then we could see the difference in Rayleigh to Lg. Since the two locations are only 70 km apart, the Rayleigh-to-Lg difference would presumably have to occur in the first 20-25 seconds. Thus it seems necessary to examine whether the P-coda are different for Degelen and Shagan in the first 20-25 seconds. Similarly, P-SV conversion could be happening further away from the source than we are modeling. It is also possible that the non-linear source effects might produce larger SV at one site versus another. These hypotheses as well as the 3-dimensional effects were not

addressed in our current experiments.

As recommendations for further work along these lines, we would suggest the following tasks:

(1) Extensions of the current finite-difference code from 2-D to 3-D to study the attenuation of body waves by 3-D heterogeneity in the crust, to test hypotheses about the generation of P coda and anisotropic P wave generation, and to model the generation of transverse Lg by explosions.

(2) Introduction of other numerical methods to explore the coupling (scattering) of modes of wave-guide regional phases such as Pg and Lg, as well as the scattering of Pn and Sn. These methods include 2-D and 3-D scattering from localized heterogeneity as well as from rough boundaries.

(3) Coupling of efficient reflectivity methods to finite difference calculations to propagate the scattered field to regional distances and to drive the finite difference responses with realistic in-coming regional phases.

(4) Investigation of scattering of fundamental and higher mode short-period Rayleigh waves by 2-D topography and shallow heterogeneity with more realistic velocity gradients near the surface.

(5) Extension of the general topographic boundary condition to include the general fluid-solid interface for the modeling of scattering at rough fluid-solid boundaries.

(6) Improvement of the polygonal free-surface boundary conditions for higher precision. One distinguishable feature of our FD code is that it allows simulations with fairly rough topography. The algorithm we use (Jih *et al.*, 1988) has first-order accuracy

consistent with the standard one-sided extrapolation formula for the flat free-surface. Even though a number of FD techniques have been proposed in recent years such as using higher-order spatial difference operator at the interior points, implicit rather than explicit scheme, etc., none of them have demonstrated significant improvement over the traditional explicit second-order scheme as long as the only available scheme implementing irregular free-surface has accuracy only of order one. This is because the overall accuracy of a FD scheme would degrade if the boundary conditions are represented by a scheme with accuracy lower than that for the interior medium. We suggest deriving an improved FD formulation of the boundary conditions so that the accuracy can be compatible with at least second order in spatial increment.

(THIS PAGE INTENTIONALLY LEFT BLANK)

APPENDIX

USER'S MANUAL OF TGALFD

A Software Package for

Seismogram Synthesis by Finite-Differences

Volume 1: fd8

Teledyne Geotech Alexandria Laboratories
314 Montgomery Street
Alexandria, Virginia 22314-1581

March 1988

Section A.0

SUMMARY

This first volume of the user's manual gives a detailed description of the current version of a sofware package, TGALFD, for generating synthetic seismograms. The program has been developed at Teledyne Geotech Alexandria Laboratories (TGAL) during the past several years. This package consists mainly of a 2-dimensional 2nd-order explicit finite-difference (FD) code which permits various source types, topographical free surface, as well as arbitrary fluctuation in (2-dimensional) medium properties. Some sample runs, free-surface boundary conditions used for topography handling, and a listing of the source code are included. The supporting routines used in analyzing the output synthetics, routines used for media generation, as well as the (machine-dependent) color snapshots display routines will be described in a follow up volume of this manual.

This FORTRAN-77 code has been run under the UNIX operation system on VAX, SUN, Celerity, and Convex computers. Users of the Center for Seismic Studies may contact Geotech for the use of this package.

Section A.1

FINITE DIFFERENCE METHOD

Wave propagation problems in seismology involve the solution of a set of differential equations in a medium in which the material properties vary in space, i.e., in the earth. The use of numerical simulations is a straightforward means for studying this kind of problem, especially when laterally-varying velocity structure or complex topographic relief is encountered. Methods such as Gaussian beam technique and ray theoretical schemes are restricted to cases where variations of the medium are much larger than the seismic wavelength. The Kirchhoff-Helmholtz integration method is useful for media with sharp interfaces, but it doesn't include the multiple scattering along the interfaces, and it is not appropriate for reflections from velocity gradients similar in extent to the seismic wavelength. Perturbation methods are applicable only for weak scattering problems. Among all numerical approaches, finite-difference (FD) and finite-element (FE) methods are not restricted to velocity variations of a particular size with respect to wavelength. FD and FE can generate synthetic seismograms for very complicated media in cases of weak/strong or multiple scattering.

FD method solves either the wave equations or the elastodynamic equations by replacing the partial derivatives in space and time by their FD approximations. When explicit FD method is used, which is the most popular FD technique to date, the wavefield of a specific time instant is solved one grid point by one grid point with nearby grid data at previous steps. For schemes that use second-order approximations to the temporal derivative, only two grid planes of displacement (or stress, velocity) must be stored to perform the updating process. Once the entire grid is updated, FD

then proceeds to compute the wavefield of next time instant until a certain preselected number of iterations is reached. The output of FD method can be snapshots of the entire grid at specific times or synthetic seismograms recorded at specific grid points.

The excellent review papers by Chin *et al.* (1984), Frankel (1988), and Stephen and Burton (1988) contain more detailed discussion of finite-difference method as well as other numerical methods used in seismology. A fairly comprehensive list of references is given at the end of this manual.

Section A.2

TGAL'S PROGRAM FD8

Revision History

Teledyne Geotech has been engaged in the development and utilization of FD code for a long time. Z. A. Der, J. Burnetti, and T. McElfresh initialized the code design in which the 2nd order explicit FD formulation (Kelly *et al.*, 1976) was adopted. They used a monochromatic P/SV planar source as well as symmetric boundary conditions to model the effects of crustal structure on teleseismic and some regional phases during 1978-1981 (Der *et al.*, 1978; Barker *et al.*, 1981). K. L. McLaughlin, T. McElfresh, and L. Anderson implemented an Ohnaka (broadband) P/SV source, a point (line) source, and absorbing boundary conditions (Clayton and Engquist, 1977; Emerman and Stephen, 1983) during 1983-1985. R.-S. Jih developed the 1st-order representation of the free-surface boundary condition to handle polygonal topography (Jih *et al.*, 1988) and coded a source-independent fundamental Rayleigh wave generation routine (Boore, 1970; Munasinghe and Farnell, 1973; Levander, 1985).

The current version of FD code **fd8** is quite different from all earlier versions (fdabc1 through fdabc6), after a series of heavy revisions was performed during 1986-1987 to allow more options to model realistic problems, even though several subroutines still retain their original names. This code has been utilized extensively by researchers at Alexandria Laboratories to study various seismological problems with funding from DARPA. The following discussion will therefore be confined to fd8

only.

   fd8 reads in control parameters from the standard input, and seismograms (time series) and error messages are written to the standard output. Snapshots of the horizontal/vertical displacements and/or strains are stored in the output file specified by the input file.

Initial Conditions

   The initial wave could be

   (+1) broadband planar P wave of Ohnaka shape,

   (-1) broadband planar S wave of Ohnaka shape,

   (+2) monochromatic planar P wave of sinusoidal shape,

   (-2) monochromatic planar S wave of sinusoidal shape,

   (+3) pure compressional (P) wave generated at a single point,

   (-3) double couple (S) point source,

   (+4) fundamental mode Rayleigh wave with Ricker wavelet shape,

   (+5) a (time series) driver file shaking a single point,

   (+6) arbitrary wavefield setting,

   (+7) broadband planar P wave of Gaussian shape,

   (-7) broadband planar S wave of Gaussian shape,

   Except for options (+5) and (+6) in which the source file or initial wavefields must be generated elsewhere in advance, **fd8** is completely self-contained to initialize the wavefields at 2 consecutive time instants to generate proper wave propagation later on.

Boundary Conditions

Absorbing boundary condition is the default for the bottom and side edges. Symmetric side boundary conditions are used only for the case of normally incident planar waves. Free surface is assumed on the top of the grid whenever a nontrivial topography is involved. All these boundary conditions can be altered by choosing appropriate input control parameters. For instance, in the case of a point source (i.e. option +/-3 or 5) without topography, there are 3 more choices by playing with incident angle:

(1) 0-degree causes all 4 edges to be absorbing,

(2) 360-degree causes symmetric top plus absorbing sides, bottom.

(3) 720-degree causes all 4 edges to be symmetric.

These extra options are meant mainly to demonstrate the effects of miscellaneous boundary conditions rather than to model realistic seismological problems.

One distinguishable feature of fd8 is that it allows simulations with fairly rough topography. The algorithm (Jih *et al.*, 1988) used here is an improved version of Ilan (1977). On the inclined free-surface, the vanishing stress conditions are implemented to a rotated coordinate system parallel to the inclined boundary, as previous works did. For each transition point on the topography where the slope changes, we use the first-order approximation of boundary conditions in a locally rotated coordinate system in which the normal axis always coincides with the bisector of the corner. These extrapolation formulae are consistent with boundary conditions to first-order accuracy in spatial increment, same as the classical one-sided explicit approximation scheme widely used for flat free-surface case. Testing results indicate that this scheme works stably for fairly complicated geometric shapes consisting of ridges and valleys with

steep and gentle slopes over a range of Poisson ratios of practical interest, thus enabling us to study more realistic problems for which the topography plays a significant role in shapin_ 'he wavefield and for which an analytical solution might not be available.

Output

The program converts numerical wavefields into character wavefields and stores these snapshots in an ASCII text file. The output wavefield could be the whole grid or only the central portion. An input parameter determines whether fixed gain or automatically adjustable scale is used in the conversion procedure.

Displacements and/or strain may be recorded as time series at any interior points for the strain or any grid points for the displacements.

The program also stores the wavefields at 2 consecutive instants and all required parameters at a prespecified rate so that it can be re-started in case the job is terminated in the middle.

Section A.3

SAMPLE INPUT FILES AND SAMPLE RUNS

Sample Input Parameter File for fd8

```
grid dimension: kw,kh
100 100
x,z spacings of the grid mesh & temporal spacing: dx,dz,dt
2 2 .2
water level: iwater (must be ≥ 2)
500
homogeneous or heterogeneous medium flag (0 or 1)
1
inLm
inMu
inRho
topography (sea-floor or ground) model: inTOP
TOP
file name for the output snapshots
movie
choose wave type: itype (see Section A.2 for legal options)
7
incidence angle (degree), i0,j0, wavelength (km) (see Remarks (a), (b))
0.01 71 2 20
option for snapshot display: component flag, AGC flag, whole (Remark (c)-(e))
# of stations to record seismograms
10
coordinates of sensors: (Remarks (f))
071 171 271 371 471 571 671 771 871 971
02 02 02 02 02 02 02 02 02 02
total number of iterations; iterations per snapshot generation
3000 200
```

Remarks:

(a) Wavelength is needed for point source, sine or Rayleigh wave,

(b) Location of source can also be used to adjust boundary conditions,

(c) 6 options for snapshot displaying are available
             h : horizontal wave fields,
             v : vertical wave fields,
             b : both horizontal & vertical wave fields,
             s : dilatational & rotational strain fields,
             m : combined displacement fields,

(d) AGC > 0 => resolution adjusted for each frame individually,

(e) size flag > 0 => whole grid will be shown,

(f) List X-coordinates of all sensors first. Negative X-coordinate means strain sensor. Y-coordinates should be in another record, and should be consistent with # of sensors above.

Sample Topography File

    10
    00 00 00 01 02 03 04 05 06 07 08 08 08 08 07 06 05 05 05 05
    EOF

Remarks:

(g) The 1st line gives the reference floor level of the topography (counted from the top of the grid). The 2nd line gives elevation with respect to the reference level at each column, *e.g.*, 03 means free surface is at 7th (= 10 - 3) row in Z-direction (counted from above), Note that the reference level must be deep enough, and each segment of the polygon must contain at least 2 sub-segments before the slope changes.

Sample Density Model File

    grid size: 20   25
    grid spacing: 0.1000   0.1000   km
    Self-Similar Medium
    Extracted from another model
    5 (dummy line)
    6 (dummy line)
    7 (dummy line)
    8 (dummy line)
        0.4927E+01 0.4982E+01 0.5106E+01 0.5123E+01 0.5128E+01
        0.5078E+01 0.5213E+01 0.5393E+01 0.5229E+01 0.5239E+01
        0.5584E+01 0.5685E+01 0.5583E+01 0.5542E+01 0.5256E+01

        ....
        EOF

Remarks:

(h) Lines 1 and 2 specify the grid size and spacings, and lines 3 and 4 are for identification purpose. Line 5 thru 8 are dummy. The remaining lines give Lame's constant at $(i,j), i=1,kw), j=1,kh$, λ, μ fields have the same format as ρ field.

Just as a simple demonstration of the capabilities as well as the limitations of our

code, figures 1 through 4 give the snapshots of wave propagation with various optional

conditions imposed.

Example A.1

Figure A.1 shows the propagation of a normally incident plane P wave through a

model with a 45° ramp on the top of grid and von Neumann (i.e. 0-slope or sym-

metric) boundary condition used on both sides. The appropriate P-S conversions and

the reflections, the diffractions satisfying Snell's law and Huygen's principle are

clearly visible in these successive snapshots taken every second. It is easy to verify

the first-order accuracy in spatial increment of our one-sided explicit representation of

the free-surface boundary conditions in this case.

Example A.2

Figure A.2 shows the snapshots of displacement fields generated by an upgoing P

wave in a grid with steep topographic configuration. The successive frames separated

by 0.125 sec show the initialization of the wave (A), P-reflection followed by S wave

starting at right (B,C), completely developed reflections from all parts of the topogra-

phy (E) and complex wavefields containing reflections, diffractions, and possibly

excited surface waves (E,F). The initial P wave has an incident angle of 20° and the

topography is a (due north 344°) cross-section of Taourirt Tan Afella Massif in south-

ern Algeria. It can be observed that the free-surface reflection is severely altered due

to scattering from the free-surface. The symmetric boundary conditions on the sides

cause some undesirable edge reflections from the left side at a later stage of the

simulation.

Example A.3

Figure A.3 uses the same topographical configuration as in Figure A.2 with absorbing boundary conditions (Clayton and Engquist, 1977; Emerman and Stephen, 1983) adopted on the sides and bottom to suppress the artificial reflections from the sides of the grid. The compressional point source in this 2-D rectangular scheme is in fact a line source in 3-D space and hence is not realistic enough in some aspects. Note that the quasi-transparent boundary conditions allow the wave to disappear into the sides and bottom of the grid.

Example A.4

Figure A.4 shows a Rayleigh wave incident on a rough topographic profile super-imposed on a grid with absorbing boundary conditions for the sides and the bottom. Figures (A) through (F) correspond to displacement wavefields at distinct times with a temporal spacing of 2 sec. Note that the high frequency scattering of Rayleigh wave is forward (McLaughlin and Jih; 1986).

Section A.4

REFERENCES

For the user's convenience, references are hereby divided into three categories:
(1) publications directly used in coding **fd8**, (2) TGAL's research that utilized **fd8** or
its earlier version, and (3) general references. All Teledyne Geotech reports are available through the National Technical Information Service.

References Directly Used In Coding fd8

Boore, D. (1970), Love waves in nonuniform wave guides: finite-difference calculations, *J. Geophys. Res.*, **75**, 1512-1527.

Clayton, R. and B. Engquist (1977), Absorbing boundary conditions for acoustic and elastic wave equations, *Bull. Seism. Soc. Am.*, **67**, 1529-1540.

Emerman, S. and R. Stephen (1983), Comment on "Absorbing boundary conditions for acoustic and elastic wave equations," by R. Clayton and B. Engquist, *Bull. Seism. Soc. Am.*, **73**, 661-665.

Jih, R.-S., K. L. McLaughlin, and Z. A. Der (1988), Free boundary conditions of arbitrary polygonal topography in a 2-D explicit elastic finite-difference scheme, *Geophysics*, **53**, 1045-1055.

Kelly, K. R., R. W. Ward, S. Treitel, and M. Alford, (1976), Synthetic seismograms: a finite-difference approach, *Geophysics*, **41**, 2-27.

Levander, A. (1985), Finite-difference calculations of dispersive Rayleigh wave propagation, *Tectonophysics*, **113**, 1-30.

Munasinghe, M. and G. Farnell (1973), Finite-difference analysis of Rayleigh wave scattering at vertical discontinuities, *J. Geophy. Res.*, **78**, 2454-2466.

Related TGAL's Research

Barker, B. W.,Z. A. Der, and C. P. Mrazek (1981), The effect of crustal structure on the regional phases P_g and L_g at the Nevada Test Site, *J. Geophys. Res.*, **86-B3**, 1686-1700.

Der, Z. A., E. M. McElfresh, C. P. Mrazek, D. P. J. Racine, B. W. Barker, A. H. Chaplin, and H. M. Sproules (1978), Results of the NTS experiment, Phase-II, *Report SDAC-TR-78-4*, Teledyne Geotech, Alexandria, VA 22314.

Jih, R.-S., and K. L. McLaughlin (1988a), Investigation of explosion generated SV Lg waves in 2-D heterogeneous crustal models by finite-difference method, *Report AFGL-TR-88-0025 (TGAL-88-01)*, Teledyne Geotech, Alexandria, VA 22314.

Jih, R.-S. and K. L. McLaughlin (1988b), Finite-difference modeling of Rayleigh wave scattering and P-SV(Lg) coupling problems, *Report AFGL-TR-88-0093 (TGAL-88-02)*, Teledyne Geotech, Alexandria, VA 22314.

Jih, R.-S., K. L. McLaughlin and Z. A. Der (1988), Free boundary conditions of arbitrary polygonal topography in a 2-D explicit elastic finite-difference scheme, *Geophysics, 53*, 1045-1055. Also Section I of *Report AFGL-TR-86-0159 (TGAL-86-03)*, Teledyne Geotech, Alexandria, VA 22314 (ADA183013).

McLaughlin, K. L., L. M. Anderson, and Z. A. Der (1985), Investigation of scattering and attenuation of seismic waves using 2-dimensional finite-difference calculations, in the *Symposium on Scattering of Waves in Random Media and Rough Surfaces*, 795-821, Varadan and Varadan editors.

McLaughlin, K. L., L. M. Anderson, and A. C. Lees (1987), Effects of geologic structure on Yucca Flats, NTS, explosion waveforms: 2-dimensional linear finite-difference simulations, *Bull. Seism. Soc. Am., 77*, 1211-1222. Also *Report AFGL-TR-86-220 (TGAL-86-04)*, Teledyne Geotech, Alexandria, VA 22314 (ADA179189).

McLaughlin, K. L. and R.-S. Jih (1986), Finite-difference simulations of Rayleigh wave scattering by 2-D rough topography, *Report AFGL-TR-86-0269 (TGAL-86-09)*, Teledyne Geotech, Alexandria, VA 22314 (ADA179190).

McLaughlin, K. L. and R.-S. Jih (1987), Finite-difference simulations of Rayleigh wave scattering by shallow heterogeneity, *Report AFGL-TR-87-0322 (TGAL-87-02)*, Teledyne Geotech, Alexandria, VA 22314.

McLaughlin, K. L. and R.-S. Jih (1988), Scattering from near-source topography: teleseismic observations and numerical 2-D explosive line sources simulations, *Bull. Seism. Soc. Am., 78*, 1399-1414. Also Section III of *Report AFGL-TR-86-0159 (TGAL-86-03)*, Teledyne Geotech, Alexandria, VA 22314 (ADA183013).

McLaughlin, K. L., R.-S. Jih, Z. A. Der, A. C. Lees (1986), The effects of near-source topography on explosion waveforms: teleseismic observations and linear finite-difference calculations, *Report AFGL-TR-86-0159 (TGAL-86-03)*, Teledyne Geotech, Alexandria, VA 22314 (ADA183013).

McLaughlin, K. L., R.-S. Jih, Z. A. Der, A. C. Lees, and L. M. Anderson (1987),
Finite-difference modeling of seismological problems in magnitude estima-
tion using body waves, surface waves and seismic source imaging, *Report
AFGL-87-0106 (TGAL-87-01)*, Teledyne Geotech, Alexandria, VA 22314
(ADA181455).

General References

Abo-Zena, A. (1979), Dispersion function computations for unlimited frequency
values, *Geophys. J. Roy. astr. Soc.*, **58**, 91-105.

Acharya, H. K., and C. R. Bentley (1878), Investigation of surface-wave dispersion
in an inhomogeneous medium by finite-difference method, *Bull. Seism. Soc.
Am.*, **68**, 1381-1386.

Alford, R. M., K. R. Kelly, and D. M. Boore (1974), Accuracy of finite-difference
modeling of the acoustic wave equations, *Geophysics*, **39**, 834-842.

Alterman, Z. S., and J. Aboudi (1970), Source of finite extent, applied force and
couple in an elastic half-space, *Geophys. J. R. astr. Soc.*, **21**, 47-64.

Alterman, Z., and F. C. Karal, Jr. (1968), Propagation of elastic waves in layered
media by finite-difference methods, *Bull. Seism. Soc. Am.*, **58**, 367-398.

Alterman, Z., and D. Loewenthal (1970), Seismic waves in a quarter and three
quarter plane, *Geophys. J. R. astr. Soc.*, **20**, 101-126.

Alterman, Z., and D. Loewenthal (1972), Computer generated seismograms, in
Methods in Computational Physics, vol. 12, 35-164.

Alterman, Z., and A. Rotenberg (1969), Seismic waves in a quarter plane, *Bull. Se-
ism. Soc. Am.*, **59**, 347-368.

Bayliss, A., K. E. Jordan, B. J. LeMesurier, and E. Turkel (1986), A fourth-order
accurate finite-difference scheme for the computation of elastic waves, *Bull.
Seism. Soc. Am.*, **76**, 1115-1132.

Bhasavanija, K. (1983), A finite difference model of an acoustic logging tool: the
borehole in a horizontally layered geologic medium, *Ph.D Thesis*, Depart-
ment of Geophysics, Colorado School of Mines, CO.

Bolt, B. A., and W. D. Smith (1976), Finite element computation of seismic
anomalies for bodies of arbitrary shape, *Geophysics*, **41**, 145-150.

Boore, D. (1972), Finite-difference methods for seismic wave propagation in
heterogeneous materials, in *Methods in Computational Physics*, vol. 11, 1-
37.

Boore, D., S. C. Harmsen, and S. Harding (1981), Wave scattering from a step change in surface topography, *Bull. Seism. Soc. Am.*, **71**, 117-125.

Bouchon, M. (1973), Effect of topography on surface motion: *Bull. Seism. Soc. Am.*, **63**, 615-632.

Bullitt, J. T. and M. N. Toksöz (1985), Three-dimensional ultrasonic modeling of Rayleigh wave propagation, *Bull. Seism. Soc. Am.*, **75**, 1087-1104.

Cerjan, C., D. Kosloff, R. Kosloff, and M. Reshef (1985), A non-reflecting boundary condition for discrete acoustic and elastic wave equations, *Geophysics*, **50**, 705-708.

Chen, T. C. and L. E. Alsop, (1979), Reflection and transmission of obliquely incident Rayleigh waves at a vertical discontinuity between two welded quarter-spaces, *Bull. Seism. Soc. Am.*, **69**, 1409-1423.

Chin, R. C. Y., G. Hedstrom, and L. Thigpen (1984), Numerical methods in seismology, *J. Comp. Phys.*, **54**, 18-56.

Clayton, R. W., Harkrider, D. G., Helmberger, D. V. (1986), Body and surface wave modeling of observed seismic events, *Report AFGL-TR-86-0021*, California Institute of Technology, Pasadena, CA (ADA169413).

Dablain, M. A. (1986), The application of high-order differencing to the scalar wave equation, *Geophysics*, **51**, 54-66.

Dougherty, M. E., and R. A. Stephen (1987), Geoacoustic scattering from seafloor features in the ROSE area, *J. Acoust. Soc. Am.*, **82**, 238-256.

Drake, L. A. (1972), Love and Rayleigh waves in nonhorizontally layered media, *Bull. Seism. Soc. Am.*, **62**, 1241-1258.

Drake, L. A. (1972), Rayleigh waves at a continental boundary by the finite element method, *Bull. Seism. Soc. Am.*, **62**, 1259-1268.

Drake, L. A. and B. A. Bolt, (1980), Love waves normally incident at a continental boundary, *Bull. Seism. Soc. Am.*, **70**, 1103-1123.

Emerman, S., W. Schmidt, and R. A. Stephen (1982), An implicit finite-difference formulation of the elastic wave equation, *Geophysics*, **47**, 1521-1526.

Fornberg, B. (1987), The pseudospectral method: comparisons with finite differences for the elastic wave equation, Geophysics, **52**, 483-501.

Frankel, A. (1988), A review of numerical experiments on seismic wave scattering, special issue on *Scattering and Attenuation of Seismic Waves* of *Pure and Applied Geophysics* (in press).

Frankel, A., and R. W. Clayton (1984), A finite-difference simulation of wave pro-
pagation in two-dimensional random media, *Bull. Seism. Soc. Am.,* **74**,
2167-2186.

Frankel, A., and R. W. Clayton (1986), Finite-difference simulation of seismic
scattering: implications for the propagation of short-period seismic waves in
the crust and models of crustal heterogeneity, *J. Geophy. Res.,* **91**, 6465-
6489.

Frankel, A., and L. Wennerberg (1987), Energy-flux model of seismic coda:
separation of scattering and intrinsic attenuation, *Bull. Seism. Soc. Am.,*
(submitted).

Fuyuki, M., and Y. Matsumoto (1980), Finite-difference analysis of Rayleigh wave
scattering at a trench, *Bull. Seism. Soc. Am.,* **70**, 2051-2069.

Fuyuki, M., and M. Nakano (1984), Finite-difference analysis of Rayleigh wave
transmission past an upward step change, *Bull. Seism. Soc. Am.,* **74**, 893-
911.

Gutowski, P., F. Hron, D. E. Wagner, and S. Treitel (1984), S*, *Bull. Seism. Soc.
Am.,* **74**, 61-78.

Harmsen, S., and S. Harding (1981), Surface motion over a sedimentary valley for
incident plane P and SV waves, Bull. Seism. Soc. Am., **71**, 665-670.

Harvey, D. J. (1981), Seismogram synthesis using normal mode superposition, the
locked mode approximation, *Geophys. J. Roy. astr. Soc.,* **66**, 37-70.

Hermance, J. F. (1982), Refined finite-difference simulations using local integral
forms: Application to telluric fields in two dimensions, *Geophysics,* **47**,
825-831.

Hill, N. R., and A. R. Levander (1984), Resonances of low-velocity layers with la-
teral variations, Bull. Seism. Soc. Am., **74**, 521-537.

Hong, M., and L. J. Bond (1986), Applications of the finite difference method in
seismic source and wave diffraction simulations, *Geophys. J. R. astr. Soc.,*
87, 731-752.

Ilan, A. (1977), Finite-difference modeling for P-pulse propagation in elastic media
with arbitrary polygonal surface, *J. Geophys.,* **43**, 41-58.

Ilan, A., L. J. Bond, and M. Spivack (1979), Interaction of a compressional im-
pulse with a slot normal to the surface of an elastic half space, *Geophys. J.
R. astr. Soc.,* **57**, 463-477.

Ilan, A., and D. Loewenthal (1976), Instability of finite difference schemes due to
boundary conditions in elastic media, *Geophys. Prospecting,* **24**, 431-453.

Ilan, A., A. Ungar, and Z. Alterman (1975), An improved representation of boundary conditions in finite-difference schemes for seismological problems, *Geophys. J. R. astr. Soc.*, 43, 727-745.

Keys, R. G. (1985), Absorbing boundary conditions for acoustic media, *Geophysics*, 50, 892-902.

Kummer, B., and A. Behle (1982), Second order finite-difference modeling of SH-wave propagation in laterally inhomogeneous media, *Bull. Seism. Soc. Am.*, 72, 793-808.

Kummer, B., A. Behle, and F. Dorau (1987), Hybrid modeling of elastic-wave propagation in 2-dimensional laterally inhomogeneous media, *Geophysics*, 52, 765-771.

Levander, A. (1985), Use of telegraphy equation to improve absorbing boundary efficiency for fourth-order acoustic wave finite-difference schemes, *Bull. Seism. Soc. Am.*, 75, 1847-1852.

Levander, A. R., Hill, N. R. (1985), P-SV resonances in irregular low-velocity surface layers, *Bull. Seism. Soc. Am.*, 75, 847-864.

Lysmer, J., and R. L. Kuhlemeyer (1969), Finite dynamic model for infinite media, *J. Eng. Mech. Div., Am. Soc. Chem. Eng.*, 95, EM4, 859-877.

Marfurt, K. J. (1984), Accuracy of finite-difference and finite-element modeling of the scalar and elastic wave equations, *Geophysics*, 49, 533-549.

Martel, L., Munasinghe, M., Farnell, G. W. (1977), Transmission and reflection of Rayleigh wave through a step, *Bull. Seism. Soc. Am.*, 67, 1277-1290.

Medwin, H., and R. P. Spaulding, Jr. (1980), The seamount as a diffracting body, in *Bottom-interfacing ocean acoustics, 421-438*, Kuperman and Jensen editors.

Oliger, J. (1976), Hybrid difference methods for the initial boundary-value problem for hyperbolic equations, *Math. Comp.*, 30, 724-738.

Ottoviani, M. (1971), Elastic wave propagation in two evenly welded quarter spaces, *Bull. Seism. Soc. Am.*, 61, 1119-1152.

Reynolds, A. C. (1978), Boundary conditions for the numerical solution of wave propagation problems, *Geophysics*, 43, 1099-1110.

Sato, Y., and K. Ishihara (1983), On the numerical calculation of wave propagation by the finite difference method, *Bull. Earthq. Res.*, 58, 163-173.

Schule, J. W. (1979), Finite element matrices for seismic surface waves in three-dimensional structures, *Bull. Seism. Soc. Am.*, 69, 1425-1437.

Schule, J. W. (1979), Love wave propagation in three-dimensional structures using finite element techniques, *Bull. Seism. Soc. Am.*, **69**, 319-328.

Schule, J. W. (1981), Seismic surface wave propagation in three dimensional finite element structures, *Bull. Seism. Soc. Am.*, **71**, 1003-1010.

Schule, J. W., and K. K. Hostettler (1987), Rayleigh wave phase velocity and amplitude values in the presence of lateral heterogeneities, *Bull. Seism. Soc. Am.*, **77**, 244-255.

Sochacki, J., R. Kubichek, J. George, W. R. Fletcher, ans S. Smithson (1987), Absorbing boundary conditions and surface waves, *Geophysics*, **52**, 60-71.

Stephen, R. A. (1983), A comparison of finite difference and reflectivity seismograms for marine models, *Geophys. J. Roy. astr. Soc.*, **72**, 39-57.

Stephen, R. A. (1984), Finite difference seismograms for laterally varying marine models, *Geophys. J. Roy. astr. Soc.*, **79**, 185-198.

Stephen, R. A. (1988), Finite-difference methods for bottom interaction problems, in the *Symposium of Computational Acoustics: Wave Propagation*, 225-238, Lee, Sternberg, and Schultz editors.

Stephen, R. A., and S. T. Bolmer (1985), The direct wave root in marine models, Bull. Seism. Soc. Am., **75**, 57-67.

Stephen, R. A., and M. Burton (1988), Finite difference solutions to the elastic wave equations with variable coefficients, *J. Comp. Phys.*, (submitted).

Stephen, R. A., F. Cardo-Casas, and C. H. Cheng (1985), Finite-difference synthetic logs, *Geophysics*, **50**, 1588-1609.

Toksöz, M. N., A. M. Dainty, and E. E. Charrette (1986), Development of ultrasonic modeling techniques for the study of seismic wave scattering due to crustal inhomogeneities, *Report AFGL-TR-86-0078*, Earth Resources Laboratory, Massachusetts Institute of Technology, MA (ADA170062).

Toksöz, M. N. (1983), Development of ultrasonic modeling techniques for the study of crustal inhomogeneities, *Report AFGL-TR-83-0070*, Earth Resources Laboratory, Massachusetts Institute of Technology, MA (ADA170062).

Ungar, A., and A. Ilan (1977), Propagation of elastic waves in vertically inhomogeneous media, *J. Geophys.*, **43**, 33-40.

Vidale, J. E., and R. W. Clayton (1986), A stable free-surface boundary condition for two-dimensional elastic finite difference wave simulation, *Geophysics*, **51**, 2247-2249.

Vidale, J. E., and D. V. Helmberger (1987), Path effects in strong motion seismology, chapter 6 in *Methods of Computational Physics*, 6, 267-319, Academic Press, New York.

Vidale, J. E., D. V. Helmberger, and R. W. Clayton (1985), Finite-difference seismograms for SH waves, *Bull. Seism. Soc. Am.*, 75, 1765-1782.

Virieux, J. (1984), SH-wave propagation in heterogeneous media: velocity-stress finite-difference method, *Geophysics*, 49, 1933-1957.

Virieux, J. (1984), P-SV wave propagation in heterogeneous media: velocity-stress finite-difference method, *Geophysics*, 51, 889-901.

Wang, C. Y. (1982), Wave theory for seismogram synthesis, Ph.D. thesis, Saint Louis University, Missouri.

Wojcik, L. W., Mak, R. (1985), A numerical study of diffraction in reentrant geologic structure, *Report AFGL-TR-85-0158*, Weidlinger Associates, Palo Alto, CA (ADA168562).

Wojcik, G. L., D. K. Vaughan, M. Barenberg, J. Mould, and M. B. Hulit (1988), Large-scale, explicit wave simulations on the Cray-2, *Applied Numerical Mathematics*, 4, 47-70.

Zahradnik, J. and L. Urban (1984), Effect of a simple mountain range on underground seismic motion, *Geophys. J. Roy. astr. Soc.*, 79, 167-183.
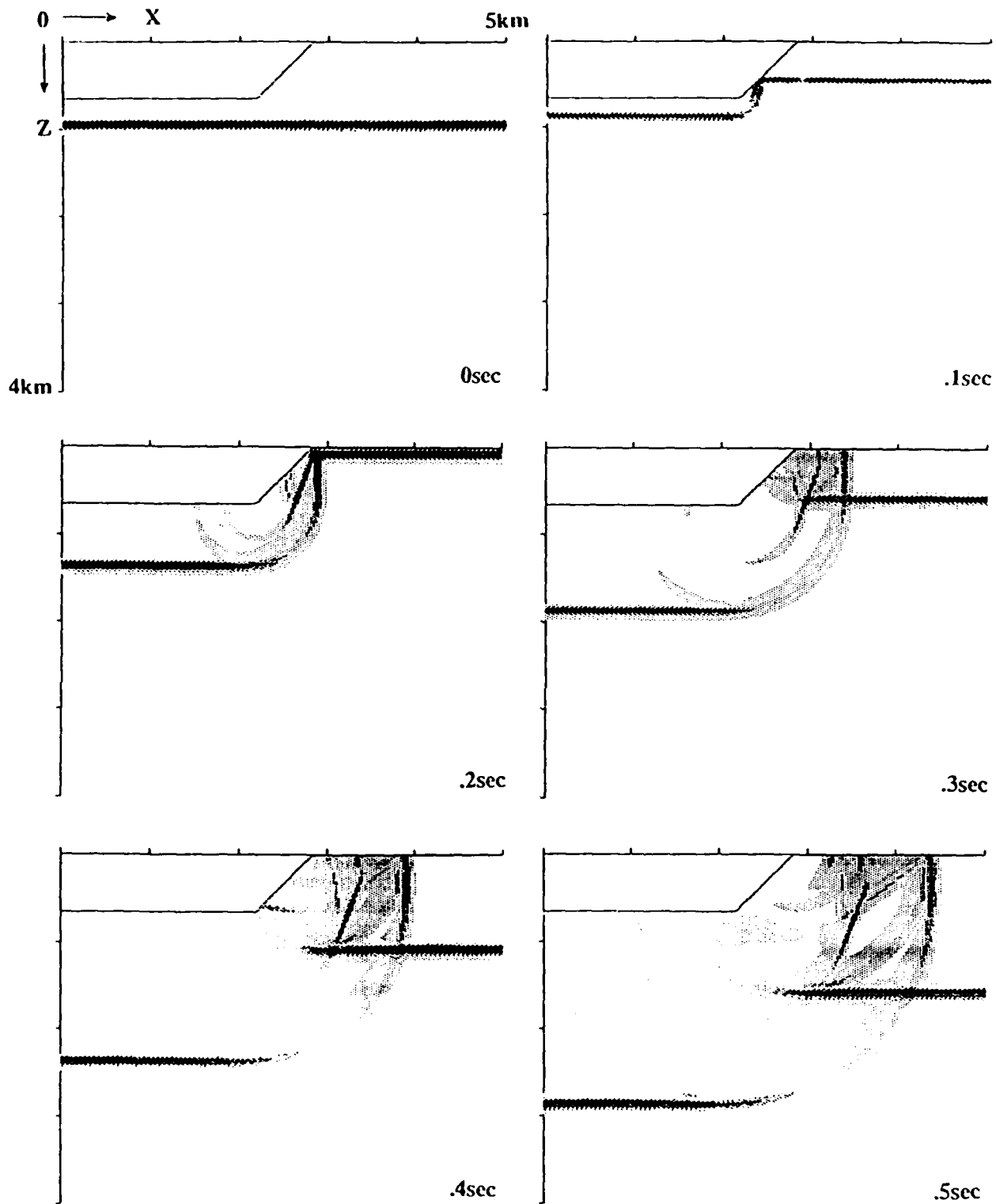
Figure A.1 The propagation of a normally incident plane P wave through a model with a 45° ramp on the top of grid and symmetric boundary condition used on both sides. The appropriate P-S conversions and the reflections, the diffractions satisfying Snell's law and Huygen's principle are clearly visible in these successive snapshots taken every second (from Jih *et al.*, 1988).

0   **6.5km**

3.9km

(A)   (B)

(C)   (D)

(E)   (F)
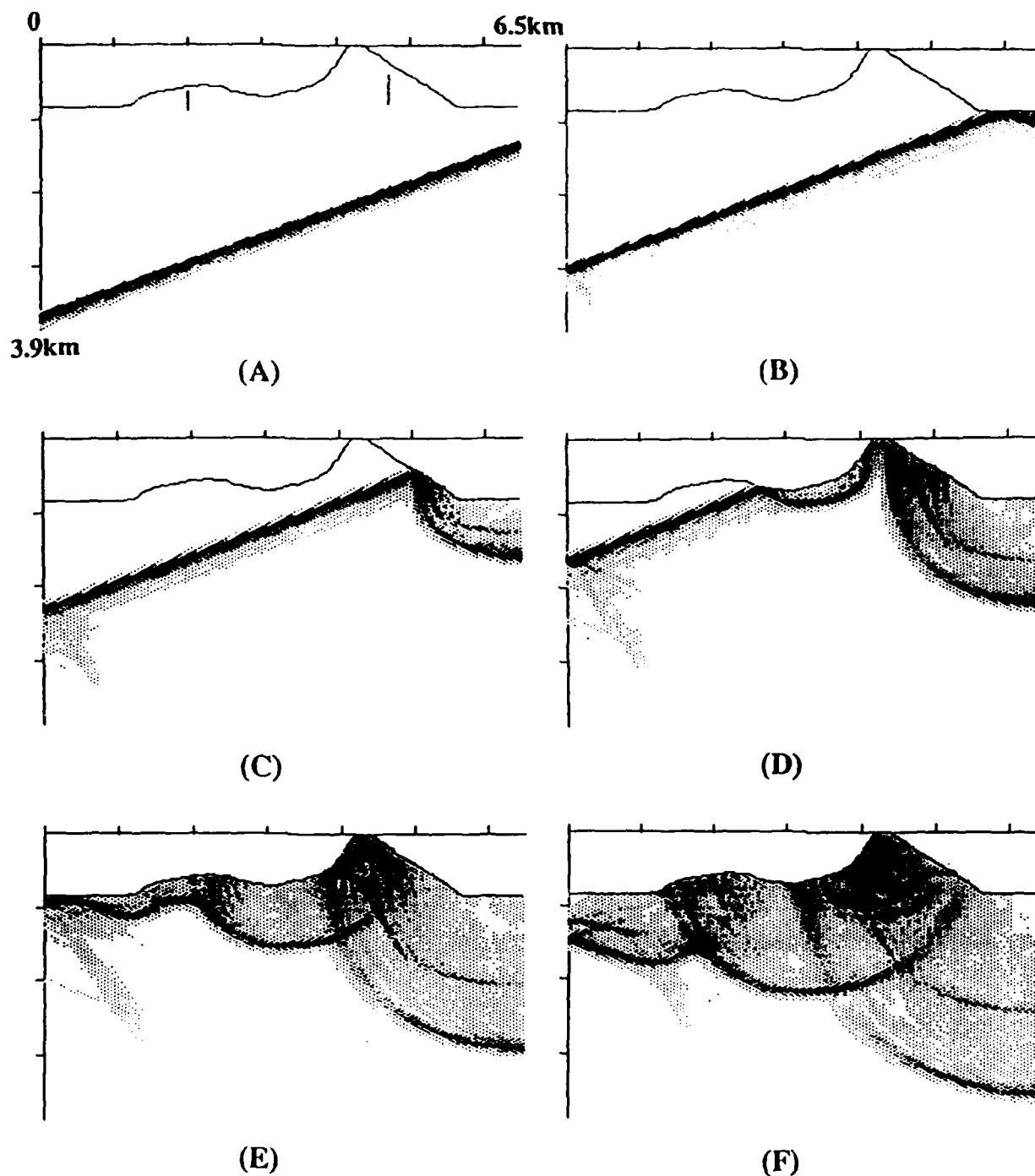
Figure A.2 The displacement fields generated by a plane P wave of incidence angle 20° in a grid with steep topographic configuration. The successive frames separated by 0.125 sec show the initialization of the wave (A), P-reflection followed by S wave starting at right (B,C), completely developed reflections from all parts of the topography (E) and complex wavefields containing reflections, diffractions and possibly excited surface waves (E,F). It can be observed that the free-surface reflection is severely altered due to scattering from the free-surface (from Jih et al., 1988).

(A)   (B)

(C)   (D)

(E)   (F)
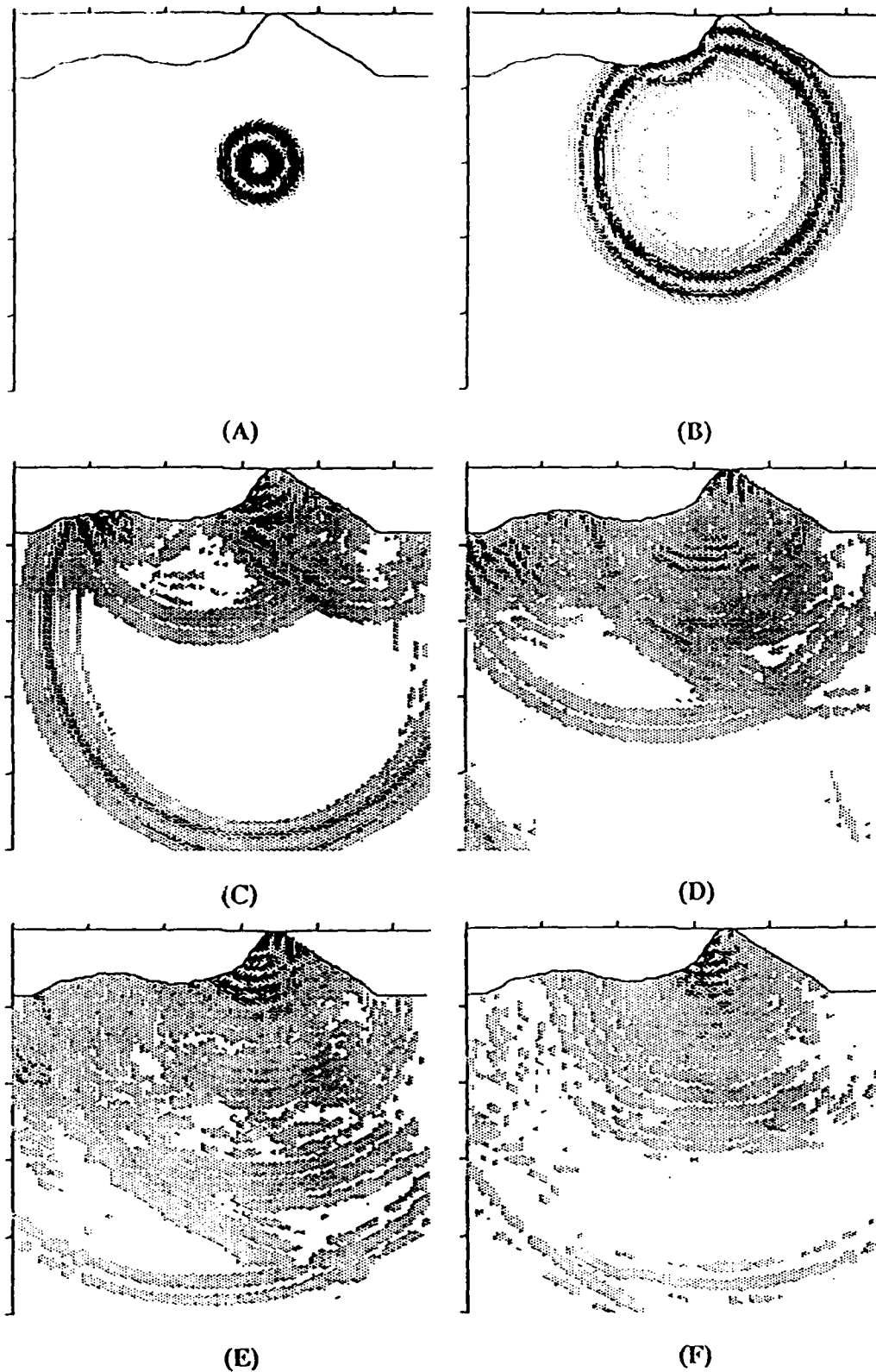
Figure A.3 Same topographical configuration as in Figure A.2 with a compressional point (line) source, and absorbing boundary conditions. Note that the quasi-transparent boundary conditions allow the wave to disappear into the sides and bottom of the grid. Snapshots are separated by 0.25 second.

(A)   (B)

(C)   (D)

(E)   (F)
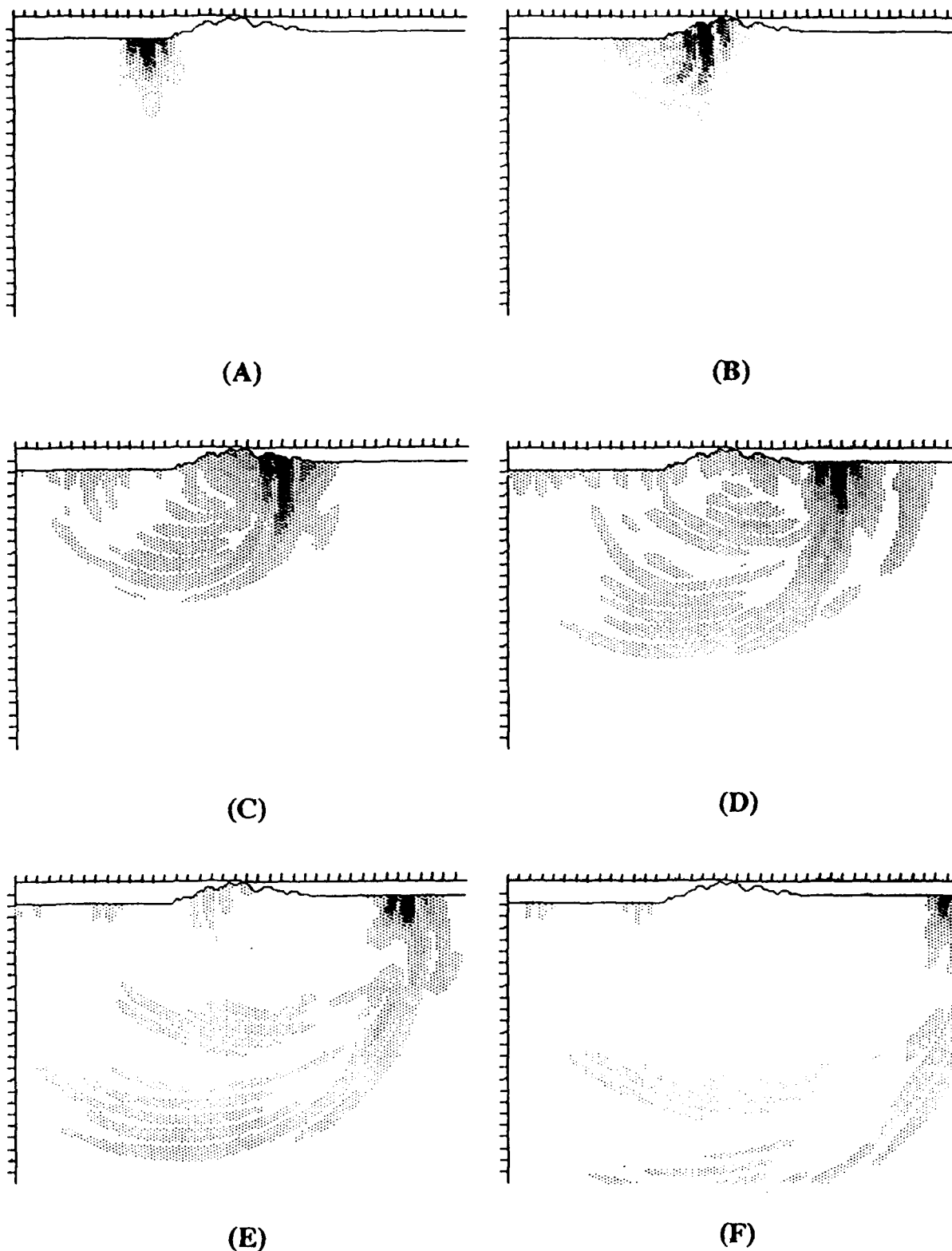
Figure A.4 Rayleigh wave incident on a rough topographic profile superimposed on a grid with absorbing boundary conditions for the sides and the bottom. Figures (A) through (F) correspond to displacement wavefields at distinct times with a temporal spacing of 2 sec. Note that the high frequency scattering of Rayleigh wave is *forward* (McLaughlin and Jih; 1986).

Professor Keiiti Aki
Center for Earth Sciences
University of Southern California
University Park
Los Angeles, CA 90089-0741

Professor Charles B. Archambeau
Cooperative Institute for Resch
   in Environmental Sciences
University of Colorado
Boulder, CO 80309

Dr. Thomas C. Bache Jr.
Science Applications Int'l Corp.
10210 Campus Point Drive
San Diego, CA 92121   (2 copies)

Dr. Douglas R. Baumgardt
Signal Analysis & Systems Div.
ENSCO, Inc.
5400 Port Royal Road
Springfield, VA 22151-2388

Dr. S. Bratt
Science Applications Int'l Corp.
10210 Campus Point Drive
San Diego, CA 92121

Dr. Lawrence J. Burdick
Woodward-Clyde Consultants
P.O. Box 93245
Pasadena, CA 91109-3245 (2 copies)

Professor Robert W. Clayton
Seismological Laboratory/Div. of
   Geological & Planetary Sciences
California Institute of Technology
Pasadena, CA 91125

Dr Karl Cogan
N. E. Research
P.O. Box 857
Norwich, VT 05055

Dr. Vernon F. Cormier
Department of Geology & Geophysics
U-45, Roon 207
The University of Conneticut
Storrs, Connecticut 06268

Dr. Zoltan A. Der
ENSCO, Inc.
5400 Port Royal Road
Springfield, VA 22151-2388

Professor John Ferguson
Center for Lithospheric Studies
The University of Texas at Dallas
P.O. Box 830688
Richardson, TX 75083-0688

Professor Stanley Flatte'
Applied Sciences Building
University of California, Santa Cruz
Santa Cruz, CA 95064

Professor Steven Grand
Department of Geology
245 Natural History Building
1301 West Green Street
Urbana, IL 61801

Professor Roy Greenfield
Geosciences Department
403 Deike Building
The Pennsylvania State University
University Park, PA 16802

Professor David G. Harkrider
Seismological Laboratory
Div of Geological & Planetary Sciences
California Institute of Technology
Pasadena, CA 91125

Professor Donald V. Helmberger
Seismological Laboratory
Div of Geological & Planetary Sciences
California Institute of Technology
Pasadena, CA 91125

Professor Eugene Herrin
Institute for the Study of Earth
 & Man/Geophysical Laboratory
Southern Methodist University
Dallas, TX 75275

Professor Robert B. Herrmann
Department of Earth & Atmospheric
      Sciences
Saint Louis University
Saint Louis, MO 63156

Professor Lane R. Johnson
Seismographic Station
University of California
Berkeley, CA 94720

Professor Thomas H. Jordan
Department of Earth, Atmospheric
 and Planetary Sciences
Mass Institute of Technology
Cambridge, MA 02139

Dr Alan Kafka
Department of Geology &
  Geophysics
Boston College
Chestnut Hill, MA 02167

Professor Leon Knopoff
University of California
Institute of Geophysics
 & Planetary Physics
Los Angeles, CA 90024

Professor Charles A. Langston
Geosciences Department
403 Deike Building
The Pennsylvania State University
University Park, PA 16802

Professor Thorne Lay
Department of Geological Sciences
1006 C.C. Little Building
University of Michigan
Ann Harbor, MI 48109-1063

Dr. Randolph Martin III
New England Research, Inc.
P.O. Box 857
Norwich, VT 05055

Dr. Gary McCartor
Mission Research Corp.
735 State Street
P.O. Drawer 719
Santa Barbara, CA 93102   (2 copies)

Professor Thomas V. McEvilly
Seismographic Station
University of California
Berkeley, CA 94720

Dr. Keith L. McLaughlin
S-CUBED,
A Division of Maxwell Laboratory
P.O. Box 1620
La Jolla, CA 92038-1620

Professor William Menke
Lamont-Doherty Geological Observatory
 of Columbia University
Palisades, NY 10964

Professor Brian J. Mitchell
Department of Earth & Atmospheric
     Sciences
Saint Louis University
Saint Louis, MO 63156

Dr. Monem Abdel-Gawad
Rockwell Internat'l Science Center
1049 Camino Dos Rios
Thousand Oaks, CA 91360

Professor Shelton S. Alexander
Geosciences Department
403 Deike Building
The Pennsylvania State University
University Park, PA 16802

Dr. Ralph Archuleta
Department of Geological
  Sciences
Univ. of California at
  Santa Barbara
Santa Barbara, CA

Dr. Muawia Barazangi
Geological Sciences
Cornell University
Ithaca, NY 14853

J. Barker
Department of Geological Sciences
State University of New York
 at Binghamton
Vestal, NY 13901

Mr. William J. Best
907 Westwood Drive
Vienna, VA 22180

Dr. N. Biswas
Geophysical Institute
University of Alaska
Fairbanks, AK 99701

Dr. G. A. Bollinger
Department of Geological Sciences
Virginia Polytechnical Institute
21044 Derring Hall
Blacksburg, VA 24061

Dr. James Bulau
Rockwell Int'l Science Center
1049 Camino Dos Rios
P.O. Box 1085
Thousand Oaks, CA 91360

Mr. Roy Burger
1221 Serry Rd.
Schenectady, NY 12309

Mr. Jack Murphy
S-CUBED
A Division of Maxwell Laboratory
11800 Sunrise Valley Drive
Suite 1212
Reston, VA 22091 (2 copies)

Professor J. A. Orcutt
Institute of Geophysics and Planetary
  Physics, A-205
Scripps Institute of Oceanography
Univ. of California, San Diego
La Jolla, CA 92093

Professor Keith Priestley
University of Nevada
Mackay School of Mines
Reno, NV 89557

Wilmer Rivers
Teledyne Geotech
314 Montgomery Street
Alexandria, VA 22314

Professor Charles G. Sammis
Center for Earth Sciences
University of Southern California
University Park
Los Angeles, CA 90089-0741

Dr. Jeffrey L. Stevens
S-CUBED,
A Division of Maxwell Laboratory
P.O. Box 1620
La Jolla, CA 92038-1620

Professor Brian Stump
Institute for the Study of Earth & Man
Geophysical Laboratory
Southern Methodist University
Dallas, TX 75275

Professor Ta-liang Teng
Center for Earth Sciences
University of Southern California
University Park
Los Angeles, CA 90089-0741

Professor M. Nafi Toksoz
Earth Resources Lab
Dept of Earth, Atmospheric and
   Planetary Sciences
Massachusetts Institute of Technology
42 Carleton Street
Cambridge, MA 02142

Professor Terry C. Wallace
Department of Geosciences
Building #11
University of Arizona
Tucson, AZ 85721

Weidlinger Associates
ATTN: Dr. Gregory Wojcik
620 Hansen Way, Suite 100
Palo Alto, CA 94304
Professor Francis T. Wu
Department of Geological Sciences
State University of new York
 At Binghamton
Vestal, NY 13901

Dr. Geza Nagy
U. California, San Diego
Dept of Ames, M.S. B-010
La Jolla, CA 92093

Dr. Jack Oliver
Department of Geology
Cornell University
Ithaca, NY 14850

Dr. Robert Phinney/Dr. F.A. Dahlen
Dept of Geological
  Geophysical Sci. University
Princeton University
Princeton, NJ 08540 (2 copies)

RADIX Systems, Inc.
Attn: Dr. Jay Pulli
2 Taft Court, Suite 203
Rockville, Maryland 20850

Professor Paul G. Richards
Lamont-Doherty Geological
 Observatory of Columbia Univ.
Palisades, NY 10964

Dr. Norton Rimer
S-CUBED
A Division of Maxwell Laboratory
P.O. 1620
La Jolla, CA 92038-1620

Professor Larry J. Ruff
Department of Geological Sciences
1006 C.C. Little Building
University of Michigan
Ann Arbor, MI 48109-1063

Dr. Alan S. Ryall, Jr.
Center of Seismic Studies
1300 North 17th Street
Suite 1450
Arlington, VA 22209-2308   (4 copies)

Dr. Richard Sailor
TASC Inc.
55 Walkers Brook Drive
Reading, MA 01867

Thomas J. Sereno, Jr.
Service Application Int'l Corp.
10210 Campus Point Drive
San Diego, CA 92121

Dr. David G. Simpson
Lamont-Doherty Geological Observ.

  of Columbia University
Palisades, NY 10964

Dr. Bob Smith
Department of Geophysics
University of Utah
1400 East 2nd South
Salt Lake City, UT 84112

Dr. S. W. Smith
Geophysics Program
University of Washington
Seattle, WA 98195

Dr. Stewart Smith
IRIS Inc.
1616 N. Fort Myer Drive
Suite 1440
Arlington, VA 22209

Rondout Associates
ATTN: Dr. George Sutton,
Dr. Jerry Carter, Dr. Paul Pomeroy
P.O. Box 224
Stone Ridge, NY 12484 (4 copies)

Dr. L. Sykes
Lamont Doherty Geological Observ.
Columbia University
Palisades, NY 10964

Dr. Pradeep Talwani
Department of Geological Sciences
University of South Carolina
Columbia, SC 29208

Dr. R. B. Tittmann
Rockwell International Science Center
1049 Camino Dos Rios
P.O. Box 1085
Thousand Oaks, CA 91360

Professor John H. Woodhouse
Hoffman Laboratory
Harvard University
20 Oxford St.
Cambridge, MA 02138

Dr. Gregory B. Young
ENSCO, Inc.
5400 Port Royal Road
Springfield, VA 22151-2388

OTHERS (FOREIGN)

Dr. Peter Basham
Earth Physics Branch
Geological Survey of Canada
1 Observatory Crescent
Ottawa, Ontario
CANADA K1A OY3

Dr. Eduard Berg
Institute of Geophysics
University of Hawaii
Honolulu, HI 96822

Dr. Michel Bouchon - Universite
  Scientifique et Medicale de Grenob
Lab de Geophysique - Interne et
  Tectonophysique - I.R.I.G.M-B.P.
38402 St. Martin D'Heres
Cedex FRANCE

Dr. Hilmar Bungum/NTNF/NORSAR
P.O. Box 51
Norwegian Council of Science,
Industry and Research, NORSAR
N-2007 Kjeller, NORWAY

Dr. Michel Campillo
I.R.I.G.M.-B.P. 68
38402 St. Martin D'Heres
Cedex, FRANCE

Dr. Kin-Yip Chun
Geophysics Division
Physics Department
University of Toronto
Ontario, CANADA M5S 1A7

Dr. Alan Douglas
Ministry of Defense
Blacknest, Brimpton,
 Reading RG7-4RS
UNITED KINGDOM

Dr. Manfred Henger
Fed. Inst. For Geosciences & Nat'l Res.
Postfach 510153
D-3000 Hannover 51
FEDERAL REPUBLIC OF GERMANY

Dr. E. Husebye
NTNF/NORSAR
P.O. Box 51
N-2007 Kjeller, NORWAY

Ms. Eva Johannisson
Senior Research Officer
National Defense Research Inst.
P.O. Box 27322
S-102 54 Stockholm
SWEDEN

Tormod Kvaerna
NTNF/NORSAR
P.O. Box 51
N-2007 Kjeller, NORWAY

Mr. Peter Marshall, Procurement
 Executive, Ministry of Defense
Blacknest, Brimpton,
 Reading FG7-4RS
UNITED KINGDOM (3 copies)

Dr. Ben Menaheim
Weizman Institute of Science
Rehovot, ISRAEL 951729

Dr. Svein Mykkeltveit
NTNF/NORSAR
P.O. Box 51
N-2007 Kjeller, NORWAY (3 copies)

Dr. Robert North
Geophysics Division
Geological Survey of Canada
1 Observatory crescent
Ottawa, Ontario
CANADA, K1A OY3

Dr. Frode Ringdal
NTNF/NORSAR
P.O. Box 51
N-2007 Kjeller, NORWAY

Dr. Jorg Schlittenhardt
Federal Inst. for Geosciences & Nat'l Res.
Postfach 510153
D-3000 Hannover 51
FEDERAL REPUBLIC OF GERMANY

University of Hawaii
Institute of Geophysics
ATTN: Dr. Daniel Walker
Honolulu, HI 96822

FOREIGN CONTRACTORS

Dr. Ramon Cabre, S.J.
c/o Mr. Ralph Buck
Economic Consular
American Embassy
APO Miami, Florida 34032

Professor Peter Harjes
Institute for Geophysik
Rhur University/Bochum
P.O. Box 102148, 4630 Bochum 1
FEDERAL REPUBLIC OF GERMANY

Professor Brian L.N. Kennett
Research School of Earth Sciences
Institute of Advanced Studies
G.P.O. Box 4
Canberra 2601
AUSTRALIA

Dr. B. Massinon
Societe Radiomana
27, Rue Claude Bernard
7,005, Paris, FRANCE (2 copies)

Dr. Pierre Mechler
Societe Radiomana
27, Rue Claude Bernard
75005, Paris, FRANCE

Dr. Ralph Alewine III
DARPA/NMRO
1400 Wilson Boulevard
Arlington, VA 22209-2308

Dr. Robert Blandford
DARPA/NMRO
1400 Wilson Boulevard
Arlington, VA 22209-2308

Sandia National Laboratory
ATTN: Dr. H. B. Durham
Albuquerque, NM 87185

Dr. Jack Evernden
USGS-Earthquake Studies
345 Middlefield Road
Menlo Park, CA 94025

U.S. Geological Survey
ATTN: Dr. T. Hanks
Nat'l Earthquake Resch Center
345 Middlefield Road
Menlo Park, CA 94025

Dr. James Hannon
Lawrence Livermore Nat'l Lab.
P.O. Box 808
Livermore, CA 94550

U.S. Arms Control & Disarm. Agency
ATTN: Dick Morrow
Washington, D.C. 20451

Paul Johnson
ESS-4, Mail Stop J979
Los Alamos National Laboratory
Los Alamos, NM 87545

Ms. Ann Kerr
DARPA/NMRO
1400 Wilson Boulevard
Arlington, VA 22209-2308

Dr. Max Koontz
US Dept of Energy/DP 331
Forrestal Building
1000 Independence Ave.
Washington, D.C. 20585

AFOSR/NP
ATTN: Colonel Jerry J. Perrizo
Bldg 410
Bolling AFB, Wash D.C. 20332-6448

HQ AFTAC/TT
Attn: Dr. Frank F. Pilotte
Patrick AFB, Florida 32925-6001

Mr. Jack Rachlin
USGS - Geology, Rm 3 C136
Mail Stop 928 National Center
Reston, VA 22092

Robert Reinke
AFWL/NTESG
Kirtland AFB, NM 87117-6008

HQ AFTAC/TGR
Attn: Dr. George H. Rothe
Patrick AFB, Florida 32925-6001

Donald L. Springer
Lawrence Livermore National Laboratory
P.O. Box 808, L-205
Livermore, CA 94550

Dr. Lawrence Turnbull
OSWR/NED
Central Intelligence Agency
CIA, Room 5G48
Washington, D.C. 20505

Dr. Thomas Weaver
Los Alamos Scientific Laboratory
Los Almos, NM 97544

AFGL/SULL
Research Library
Hanscom AFB, MA 01731-5000 (2 copies)

Secretary of the Air Force (SAFRD)
Washington, DC 20330
Office of the Secretary Defense
DDR & E
Washington, DC 20330

HQ DNA
ATTN: Technical Library
Washington, DC 20305

Director, Technical Information
DARPA
1400 Wilson Blvd.
Arlington, VA 22209

AFGL/XO
Hanscom AFB, MA 01731-5000

Dr. W. H. K. Lee
USGS
Office of Earthquakes, Volcanoes,
  & Engineering
Branch of Seismology
345 Middlefield Rd
Menlo Park, CA 94025

Dr. William Leith
USGS
Mail Stop 928
Reston, VA 22092

Dr. Richard Lewis
Dir. Earthquake Engineering and
  Geophysics
U.S. Army Corps of Engineers
Box 631
Vicksburg, MS 39180

Dr. Robert Masse'
Box 25046, Mail Stop 967
Denver Federal Center
Denver, Colorado 80225

R. Morrow
ACDA/VI
Room 5741
320 21st Street N.W.
Washington, D.C. 20451

Dr. Keith K. Nakanishi
Lawrence Livermore National Laboratory
P.O. Box 808, L-205
Livermore, CA 94550 (2 copies)

Dr. Carl Newton
Los Alamos National Lab.
P.O. Box 1663
Mail Stop C335, Group E553
Los Alamos, NM 87545

Dr. Kenneth H. Olsen
Los Alamos Scientific Lab.
Post Office Box 1663
Los Alamos, NM 87545

Howard J. Patton
Lawrence Livermore National Laboratory
P.O. Box 808, L-205
Livermore, CA 94550

Mr. Chris Paine
Office of Senator Kennedy
SR 315
United States Senate

Washington, D.C. 20510

AFGL/LW
Hanscom AFB, MA 01731-5000

DARPA/PM
1400 Wilson Boulevard
Arlington, VA 22209

Defense Technical
 Information Center
Cameron Station
Alexandria, VA 22314
(5 copies)

Defense Intelligence Agency
Directorate for Scientific &
  Technical Intelligence
Washington, D.C. 20301

Defense Nuclear Agency/SPSS
ATTN: Dr. Michael Shore
6801 Telegraph Road
Alexandria, VA 22310

AFTAC/CA (STINFO)
Patrick AFB, FL 32925-6001

Dr. Gregory van der Vink
Congress of the United States
Office of Technology Assessment
Washington, D.C. 20510

Mr. Alfred Lieberman
ACDA/VI-OA'State Department Building
Room 5726
320 - 21St Street, NW
Washington, D.C. 20451.